Accepted Article

J Musculoskelet Neuronal Interact 2022

Journal of Musculoskeletal and Neuronal Interactions JMNI

Original Article

Time course changes to structural, mechanical and material properties of bone in rats after complete spinal cord injury

Jonathan A. Williams[1], Carmen Huesa[2], Mikael J. Turunen[3], James A. Oo[4,5], Oskars Radzins[6,7], Wilf Gardner[4], James F.C. Windmill[8], Hanna Isaksson[9], K. Elizabeth Tanner[6,10,11], John S. Riddell[4], Sylvie Coupaud[1]

[1]Department of Biomedical Engineering, Wolfson Building, University of Strathclyde, Glasgow, UK;
[2]Centre for Musculoskeletal Science, University of the West of Scotland, Paisley, UK;
[3]Department of Applied Physics, University of Eastern Finland, Kuopio, Finland;
[4]Institute of Neuroscience and Psychology, College of Medical, Veterinary and Life Sciences, University of Glasgow, UK;
[5]Now at Institute for Cardiovascular Physiology, Goethe University, Frankfurt am Main, Germany;
[6]Biomedical Engineering Division, James Watt School of Engineering, James Watt South Building University of Glasgow, Glasgow, UK;
[7]Now at Department of Orthodontics, Institute of Stomatology, Riga Stradins University, Latvia;
[8]Department of Electronic and Electrical Engineering, Royal College Building, University of Strathclyde, Glasgow, UK;
[9]Department of Biomedical Engineering, Lund University, Sweden;
[10]Lund University, Faculty of Medicine, Department of Clinical Sciences Lund, Orthopedics, Sweden;
[11]Now at School of Engineering and Materials Science and Institute of Bioengineering, Queen Mary University of London, Mile End Road, London, UK

Abstract

Objective: Characterise the spatiotemporal trabecular and cortical bone responses to complete spinal cord injury (SCI) in young rats. **Methods:** 8-week-old male Wistar rats received T9-transection SCI and were euthanised 2-, 6-, 10- or 16-weeks post-surgery. Outcome measures were assessed using micro-computed tomography, mechanical testing, serum markers and Fourier-transform infrared spectroscopy. **Results:** The trabecular and cortical bone responses to SCI are site-specific. Metaphyseal trabecular BV/TV was 59% lower, characterised by fewer and thinner trabeculae at 2-weeks post-SCI, while epiphyseal BV/TV was 23% lower with maintained connectivity. At later-time points, metaphyseal BV/TV remained unchanged, while epiphyseal BV/TV increased. The total area of metaphyseal and mid-diaphyseal cortical bone were lower from 2-weeks and between 6- and 10-weeks post-SCI, respectively. This suggested that SCI-induced bone changes observed in the rat model were not solely attributable to bone loss, but also to suppressed bone growth. No tissue mineral density differences were observed at any time-point, suggesting that decreased whole-bone mechanical properties were primarily the result of changes to the spatial distribution of bone. **Conclusion:** Young SCI rat trabecular bone changes resemble those observed clinically in adult and paediatric SCI, while cortical bone changes resemble paediatric SCI only.

Keywords: Bone Mechanical Properties, Fourier-transform Infrared Spectroscopy, microCT, Osteoporosis, Spinal Cord Transection

Carmen Huesa was supported by the Versus Arthritis early career fellowship (grant no. 22483). The remaining authors have nothing to declare.

Corresponding author: Jonathan Anthony Williams, Department of Biomedical Engineering, Wolfson Building, University of Strathclyde, 106 Rottenrow East, Glasgow, G4 ONW, United Kingdom
ORCiD number 0000-0002-9828-4886
E-mail: jonathan.williams@strath.ac.uk

Edited by: G. Lyritis
Accepted 2 January 2022

Introduction

Injury to the spinal cord can result in paralysis below the level of injury. A secondary complication, triggered by the removal of muscle-driven dynamic bone stimulation and the neurological insult itself, is the development of a rapid and severe osteoporosis in the bones of the paralysed lower extremities (sublesional bone loss)[1]. This severe

deterioration of both bone quantity and microarchitecture means that patients with spinal cord injury (SCI) are at a significantly higher risk of fragility fractures in the lower extremities than the able-bodied population, particularly around the knee (distal femur and proximal tibia), in the trabecular-rich epiphyseal and metaphyseal compartments[2]. For individuals with a complete SCI, fracture incidence increases with time, from 1% in the first 12-months, to 4.6% per year at 20-years post-injury[3]. Long term follow-up suggests that up to half of all patients with SCI will sustain at least one fragility fracture, with an average time to first fracture of 8.9 years post-SCI[3].

Rat models are commonly used to characterise and understand the mechanisms of SCI-induced osteoporosis. The majority of previous studies have used a single-time point, studying only the acute (less than 6-week phase)[4–10] or more chronic phase of the injury[11]. Most studies have used young, skeletally immature rats (10-week-old or younger[4–9,12,13]), in which there is continuing longitudinal and appositional bone growth. Most clinical cases of traumatic SCI occur in skeletally mature humans[14] and whether skeletally immature rats are a good model of clinical SCI-induced osteoporosis has not been investigated.

A major variable in all these rat studies is the type of SCI. Both contusion[6,10,11,15,16] and transection[4,5,7–9,12] type injuries have been used. Contusion injuries are always incomplete injuries, always accompanied by recovery of motor function. This recovery is faster and more extensive than in human SCI. The recovery of motor function in the model confounds the investigation of disuse related osteoporosis. A transection injury, which completely severs the spinal cord, results in complete and permanent loss of volitional movement. This avoids the confounding effect of motor recovery in incomplete models and makes it more suitable for studying SCI-induced osteoporosis.

Several time course studies have been performed. Peng et al., (2020)[17] and Minematsu et al. (2014)[9] examined changes in metaphyseal trabecular microstructure only, for the femur and tibia, respectively, during the first week and first 5-weeks after transection SCI, respectively, in 8-week-old male rats. Otzel et al. (2019)[16] evaluated the trabecular and cortical bone deterioration over 3-months after contusion SCI in 16-week-old rats. Despite the trabecular-rich epiphyseal and metaphyseal compartments being most common to fracture clinically, so far only one single-time point rat study has examined the epiphysis[11].

In this study, we used 8-week-old male rats that received a T9-transection SCI, with age-matched sham-operated controls. The motivation was to assess the suitability of a young rat model in mimicking the SCI-induced osteoporosis observed in human SCI, by characterising the temporal changes produced by a transection SCI on the microarchitecture of several different distal femoral trabecular and cortical bone site.

Material and Methods

Animals

Sixty-four male Wistar rats weighing 200±4g (approximately 7-weeks-old) were acquired from Harlan Laboratories, Loughborough, UK. Rats were housed in pairs, in a temperature-controlled room under a 12-hour light-dark cycle, with *ad libitum* access to food and water. All experimental procedures were approved by the Ethical Review Panel of the University of Glasgow and carried out in accordance with the Animals (Scientific Procedures) Act 1986.

Experimental Design

Rats were randomly assigned to SCI or SHAM groups (n=32 per group). Subsets of rats were euthanised at 2-, 6-, 10- or 16-weeks post-surgery (n=8 per group) by anaesthetic overdose (Euthatal, Merial Animal Health Ltd, Harlow, UK). Body mass was measured daily for the first week post-surgery, subsequently a weekly measurement was performed. Blood samples were acquired at the time of sacrifice via the descending aorta. Serum was separated and stored at -80°C. Right gastrocnemius muscles (both medial and lateral heads), biceps and triceps muscles and tibiae and humeri and left and right femora were dissected and weighed. Femoral length was measured parallel to the shaft between the femoral head and condyles using digital callipers. Femurs were wrapped in PBS-soaked gauze and stored at -20°C for micro-computed tomography (μCT) and subsequent destructive mechanical testing.

Surgery and Postoperative Care

Following 1-week of acclimatisation (8-week-old) rats underwent transection of the spinal cord at thoracic level T9. Surgery and postoperative care were carried out as previously described[18]. Briefly, a laminectomy was performed at the T9-T10 level in anesthetised rats. In SHAM rats, the wound was immediately closed. In SCI rats, a transection injury was produced by making a small hole in the dura and cutting the spinal cord transversely at two locations, approximately 1mm apart. Rats received buprenorphine (0.05 mg/kg s.c.) and carprofen (5 mg/kg s.c.) the morning of and morning after surgery. Saline (3–5 ml s.c.) and enrofloxacin (5 mg/kg s.c.) were given for 3- and 7-days post-surgery for SHAM and SCI, respectively. The bladders of SCI rats were expressed 3-times per day until spontaneous voiding returned.

μCT analysis

Right femurs were scanned using μCT (Bruker SkyScan 1172 scanner, Kontich, Belgium) at 6.9 μm isotropic voxel size, as described previously[18]. 2D global morphometry was performed on the most distal 60% of the femur (Online Resource 1), which guided the volume of interest (VOI)

selection for 3D morphometric analysis. A percentage of bone length-based approach was used to define the VOIs. Two trabecular VOIs, both only containing secondary spongiosa were selected, a metaphyseal (81–85% bone length from the proximal end) and epiphyseal (93–97% bone length from the proximal end) VOI. Two cortical VOIs were also selected, a metaphyseal (81–85% bone length from the proximal end) and mid-diaphyseal (58–62% bone length from the proximal end) VOI, as previously described[18]. Trabecular measures included: bone volume fraction (BV/TV), trabecular thickness (Tb.Th), trabecular number (Tb.N), trabecular separation (Tb.Sp), specific bone surface (BS/BV), connectivity density (Conn.D) as described by Bouxsein et al. (2010)[19], trabecular pattern factor (Tb.Pf)[20], and the un-plate index (uPi), which is the ratio of a structure's Tb.Th to the thickness derived assuming a 2D plate-based model, indicating departure from an ideal plate morphology[21]. Cortical measures included: average cortical thickness (Ct.Th), cortical bone area (Ct.Ar), total cross-sectional area inside the periosteal envelop (Tt.Ar), medullary area (Ma.Ar), cortical area fraction (Ct.Ar/Tt.Ar), polar moment of area (J), specific cortical bone surface (BS/BV) and eccentricity (Ecc)[22]. Trabecular volumetric bone mineral density (vBMD) and cortical tissue mineral density (TMD) were determined after calibration using two 4mm diameter hydroxyapatite calibration phantoms, with densities of 0.25 and 0.75 g cm^{-3}.

Mechanical Testing

Subsequent to µCT scanning, right femurs underwent loading to failure in a three-point bend test in the posterior-anterior configuration (with the posterior surface in tension) at 1mm s^{-1}, using a servohydraulic testing machine with a 2kN load cell (Zwick/Roell z2.0, August-Nagel-Strasse 11, Ulm, Germany). Load and actuator displacement were digitally recorded at a sampling rate of 100 Hz, using testXpert II (Version 3.61) software. A 15 mm span length was used for 6-, 10- and 16-weeks post-surgery femurs, while span length was reduced to 13mm for 2-week groups (to avoid the distal growth plate of these smaller bones resting on one of the outer supports). Force-displacement data were converted to moment (M=FL/4) and normalised displacement (d'=12d/L2), respectively, to account for differences in span length[23]. The whole-bone mechanical properties of rigidity, ultimate moment, and energy-to-fracture were obtained. The tissue-level mechanical properties of elastic modulus and ultimate stress were calculated from the equations of beam theory[24]. Left femurs underwent a torsion test, using a servohydraulic testing machine (Instron 8511 load frame, High Wycombe, UK, MTS Series 793 controller), as previously described by Bosemark et al. (2014)[25], in which the proximal end was fixed, and the distal end was rotated at 6° s^{-1} until failure. The whole-bone mechanical properties of rotational stiffness, ultimate torque and energy-to-fracture were obtained, and the tissue-level mechanical properties of shear (rigidity) modulus and ultimate shear stress were calculated. Furthermore, the whole-bone mechanical properties derived from three-bend and torsion testing were adjusted for body mass using the linear regression method[23].

Serum Measurements

Serum markers of bone formation and resorption were measured from each rat using Rat/Mouse Procollagen type 1 N-terminal propeptide (P1NP) and RatLaps™ C-terminal telopeptide of type I collagen (CTX-I) enzyme immunoassay kits (Immunodiagnostic Systems, Tyne & Wear, UK), respectively at the time of death. The assays were performed following manufacturer's instructions.

Fourier Transform Infrared (FTIR) Spectroscopy

Mid-diaphyseal bone from the proximal end of torsion-tested 10-week post-surgery SHAM (n=7) and SCI (n=8) femora were prepared for a preliminary FTIR spectroscopy study through dehydration and embedding in PMMA (Online Resource 2). Longitudinal sections of 3 µm were cut centrally and were placed on BaF_2 windows. Measurements were done at the B22 beamline at Diamond Light Source (Didcot, UK), using Endstation 2 with a Bruker 3000 microscope and Vertex 80V Fourier Transform IT Interferometer, with an MCT detector and 36x objective. Spectra for each measurement point were collected using a 10 x 10 $µm^2$ beam size and spectral resolution of 4 cm^{-1} with averaging of 32 scans, in the range of 500-4000 cm^{-1}. Calibration of the system was performed before every measurement session following the manufacturer's instructions. The background was measured after every 10 sample measurements. Based on the light microscope image, measurements were done as line scans with 5 µm spacing over the cortex, resulting in 124±56 (mean ± SD) data points per line. For each rat, two sections were measured, each with three lines across the mid-diaphyseal cortex in the posterior region (Online Resource 2). Measurements were performed away from the failure site. Mineral-to-matrix ratio (phosphate peak [900-1200 cm^{-1}] / amide I peak [1585-1720 cm^{-1}])[26], acid phosphate substitution (APS, 1127/1096 cm^{-1})[27], and collagen maturity (XLR, 1660/1690 cm^{-1})[28] were determined after removing the spectrum of the embedding media using pre-defined methods (MATLAB, v 7.6.0 MathWorks Inc. Natick USA)[29]. Linear baseline corrections were performed for each peak area measurement using the peak's wavenumber region (e.g. 900-1200 cm^{-1} for phosphate). The mean as well as the spatial heterogeneity[30] were calculated for each parameter for each rat and compared between SHAM and SCI.

Statistical analysis

Group (SCI, SHAM) and time (2-, 6-, 10- and 16-weeks post-surgery) main effects and interactions were determined with two-way [2×4] ANOVAs for all outcome

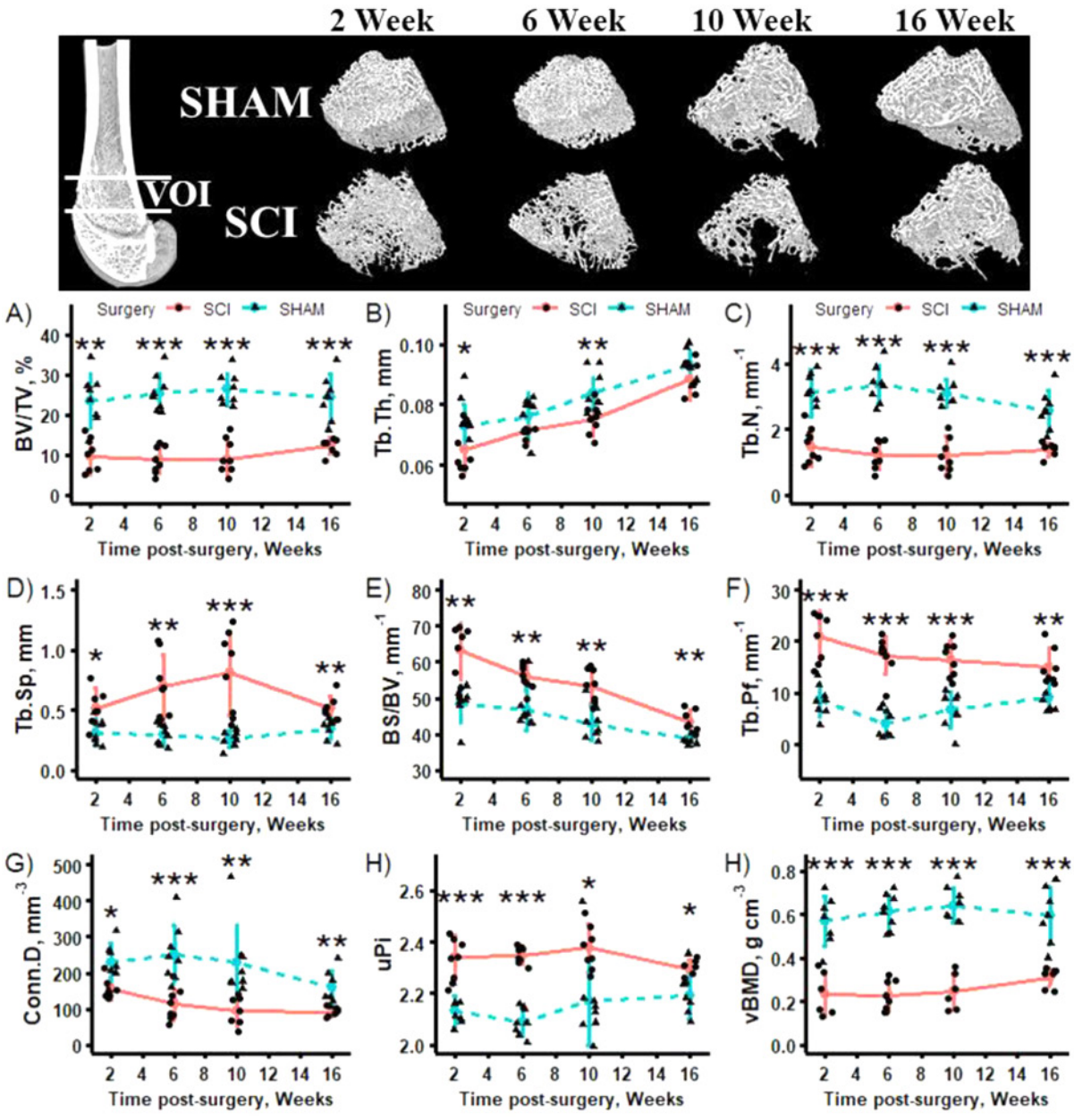

Figure 1. Representative μCT-based images of metaphyseal trabecular architecture and mean morphometric outcome measures for 2-, 6-, 10- and 16-weeks post-surgery SCI and SHAM groups (all n=8). Data shown as mean ± SD. *, ** and *** indicate p<0.05, p<0.01 and p<0.001, respectively, for SCI versus SHAM at the same post-surgical timepoint.

measures, with Tukey's post hoc tests for multiple comparisons among groups. Additionally, four targeted Student's t-tests for independent samples were performed *a priori* to determine differences between SCI and SHAM groups at the same post-surgery time point. The Wilcoxon signed ranks test was performed to study the differences between epiphyseal vs. metaphyseal trabecular bone compartments for the 2-week post-surgery SHAM group only. Significance was defined as p<0.05.

Results

Body mass at time of surgery was similar between SCI (235±2g) and SHAM (232±2g) groups. Due to growth in the rat model, between time of surgery and 16-weeks post-surgery there was a 53% and 86% (both p<0.001) increase in body mass for SCI and SHAM, respectively (Online Resource 3). From day 3 post-surgery SCI body mass was lower than SHAM (p<0.05). The sublesional gastrocnemius, femoral and

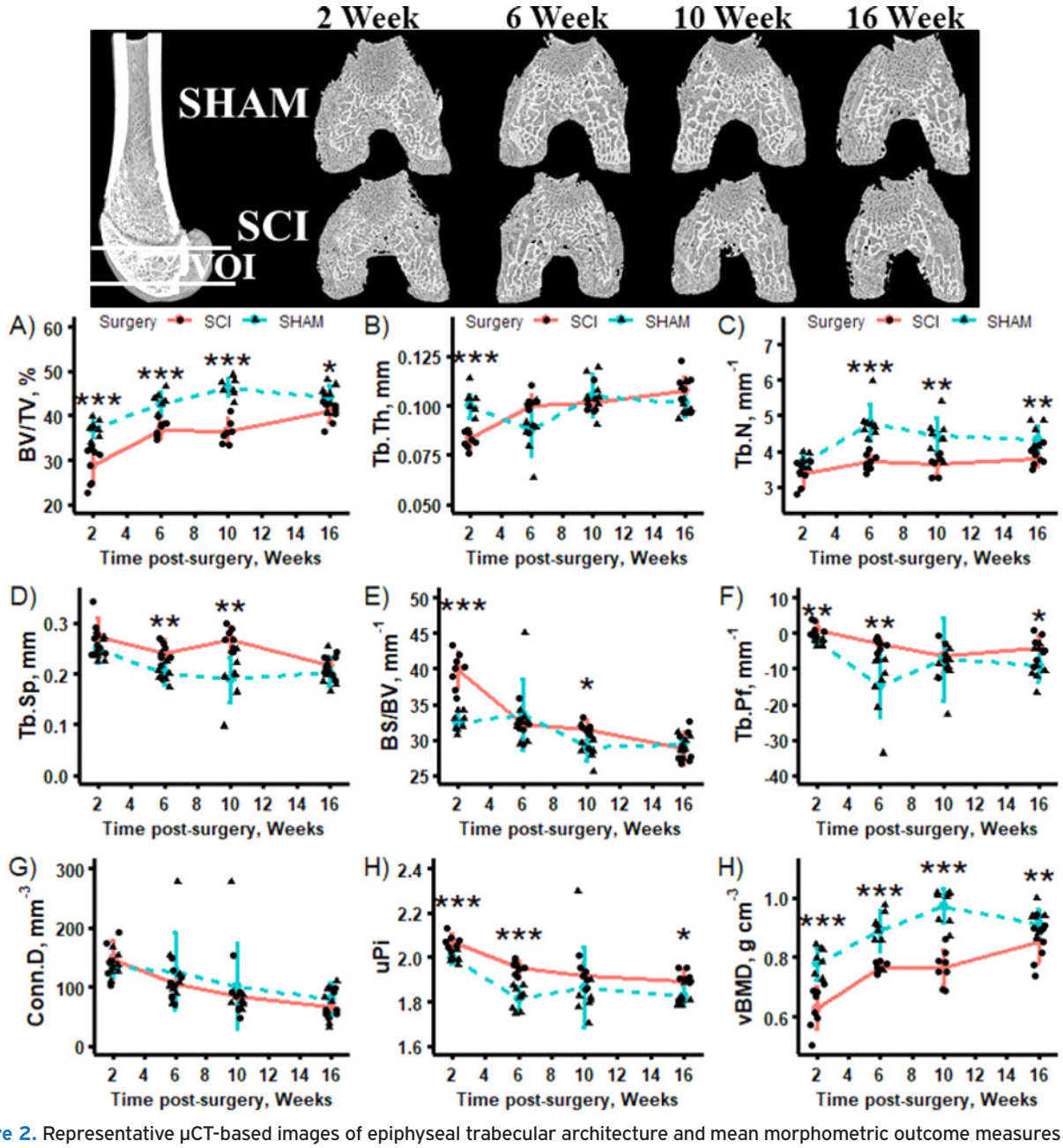

Figure 2. Representative μCT-based images of epiphyseal trabecular architecture and mean morphometric outcome measures for 2-, 6-, 10- and 16-weeks post-surgery SCI and SHAM groups (all n=8). Data shown as mean ± SD. *, ** and *** indicate p<0.05, p<0.01 and p<0.001, respectively, for SCI versus SHAM at the same post-surgical timepoint.

tibial masses in SCI were significantly lower at all time points (2-, 6-, 10- and 16-weeks) post-surgery (p<0.001) (Online Resource 4). By 2-weeks post-surgery gastrocnemius mass was 36% (p<0.001) lower in SCI. Femoral bone mass changes lagged behind muscle mass changes at 2-weeks post-surgery, where an 8% (p<0.001) lowering was observed in SCI. By 6-weeks the difference increased to 20% (p<0.001), which was maintained at later time points. In contrast, for the upper extremities, supralesional biceps, triceps and humeri masses were only significantly lower (p<0.05) at 10-weeks post-surgery in SCI (Online Resource 5). Femoral length was unaffected by SCI-induced osteoporosis. A 15% and 16% increase in femoral length was observed between 2- and 16-weeks post-surgery for SCI and SHAM, respectively (Online Resource 6).

μCT Analysis of Metaphyseal Trabecular Morphometry

Representative distal femoral metaphyseal secondary spongiosa VOIs and morphometric measures are shown in

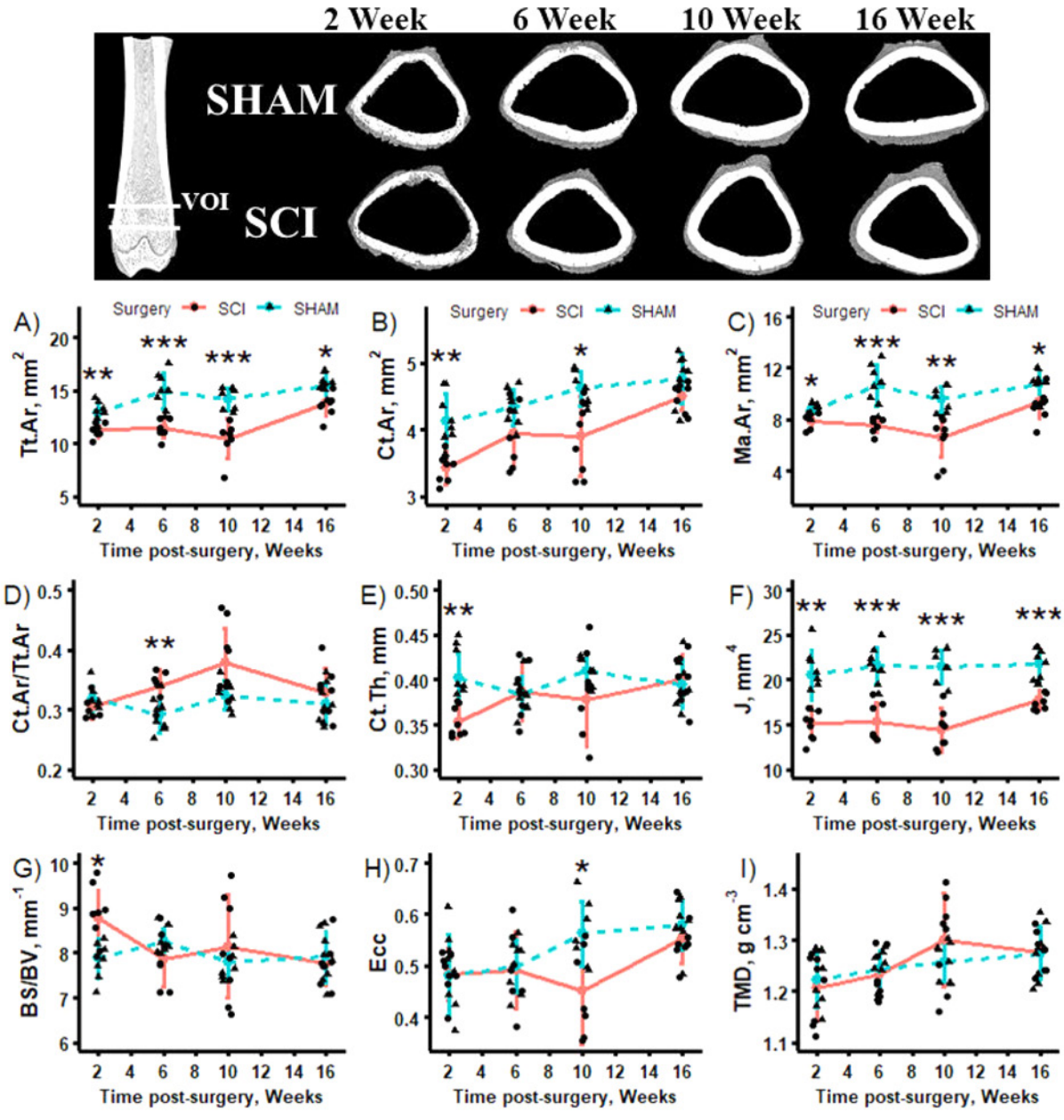

Figure 3. Representative µCT-based images of distal metaphyseal cortical bone (81-85% bone length) and mean morphometric outcome measures and tissue mineral density for 2-, 6-, 10- and 16-weeks post-surgery SCI and SHAM groups (all n=8). Data shown as mean ± SD. *, ** and *** indicate p<0.05, p<0.01 and p<0.001, respectively, for SCI versus SHAM at the same post-surgical timepoint.

Figure 1. Group main effects indicated that SCI exhibited lower BV/TV, vBMD, Tb.N and Conn.D, as well as higher Tb.Sp, BS/BV, Tb.Pf and uPi. Time main effects indicated higher Tb.Th and lower BS/BV, Conn.D and Tb.Pf (SCI only) for later time points post-surgery in SHAM and SCI groups.

At 2-weeks post-surgery, SCI experienced 58% and 59% lower metaphyseal vBMD and BV/TV (both p<0.001), respectively, compared to SHAM. The lowering of BV/TV was characterised by a 53% and 15% lower Tb.N (p<0.001) and Tb.Th (p<0.01), respectively, with 65% higher Tb.Sp (p<0.05) compared to SHAM. These structural changes led to 30% higher BS/BV (p<0.01), 32% lower Conn.D (p<0.05) and a 145% and 10% higher Tb.Pf and uPi (both p<0.001), respectively in SCI compared to SHAM. At all later time points assessed post-SCI, no further vBMD or BV/TV changes were observed for SHAM or SCI. Despite this, further microstructural changes occurred. Tb.Th

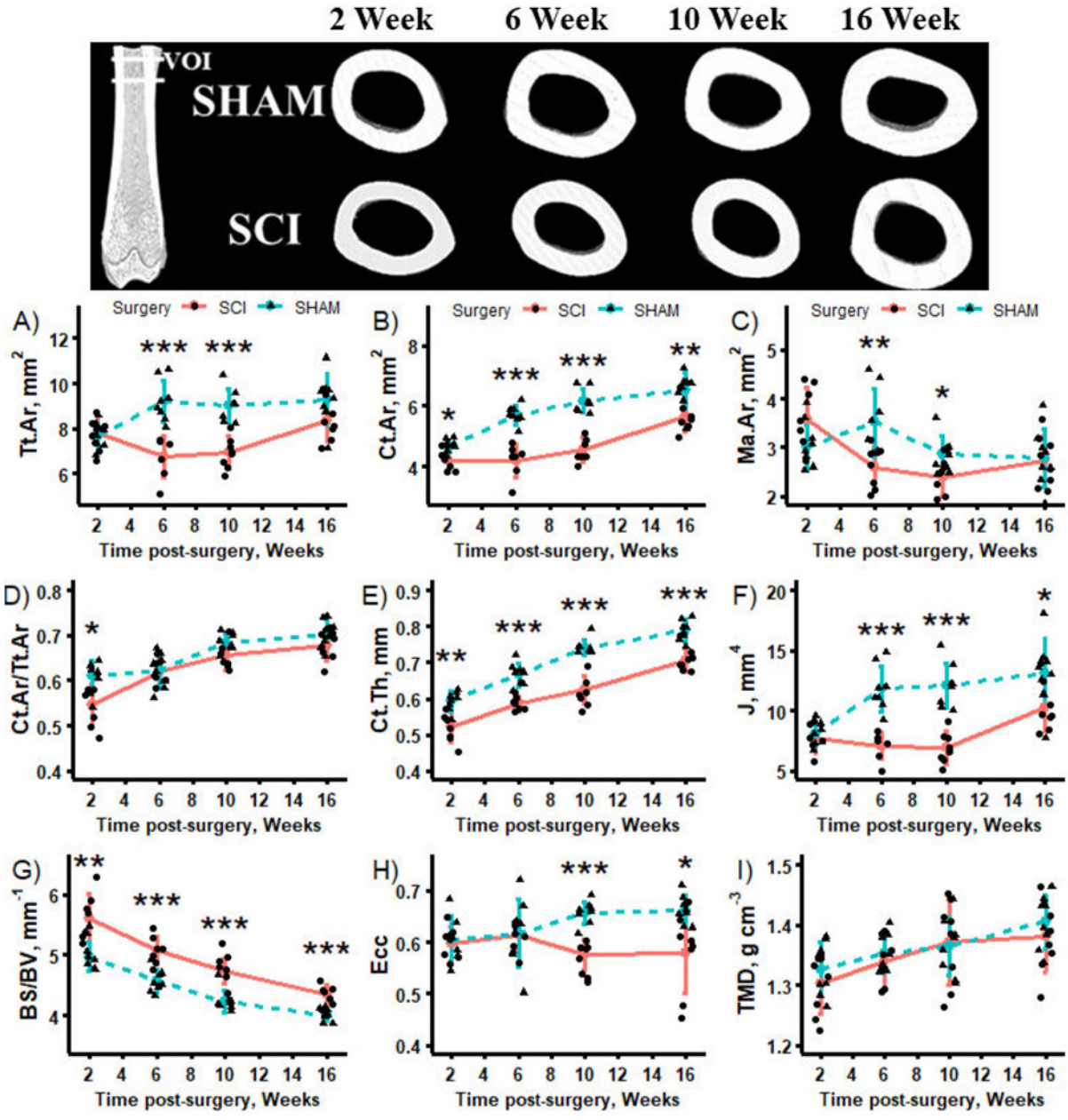

Figure 4. Representative µCT-based images of mid-diaphyseal cortical bone (58-62% bone length) and mean morphometric outcome measures and tissue mineral density for 2-, 6-, 10- and 16-weeks post-surgery SCI and SHAM groups (all n=8). Data shown as mean ± SD. *, ** and *** indicate p<0.05, p<0.01 and p<0.001, respectively, for SCI versus SHAM at the same post-surgical timepoint.

increased monotonically between 2- and 16-weeks for SHAM and SCI (both p<0.001), by 16-weeks post-surgery no difference existed between groups, while Tb.N remained relatively constant. BS/BV and Conn.D decreased between 2- and 16-weeks for SHAM and SCI (p<0.05). Tukey's post hoc time comparisons for SHAM and SCI groups are provided in Online Resources 7, 8, 9, 10, 11 and 12, for all assessed trabecular, cortical and mechanical outcome measures.

µCT Analysis of Epiphyseal Trabecular Morphometry

Representative distal femoral epiphyseal spongiosa VOIs and morphometric measures are shown in Figure 2. A comparison of 2-week post-surgery SHAM metaphyseal secondary spongiosa and epiphyseal spongiosa VOIs showed that the epiphyseal VOIs contained higher BV/TV, characterised by higher Tb.Th (both p<0.001), but lower Conn.D and BS/BV (both p<0.001). Group main effects

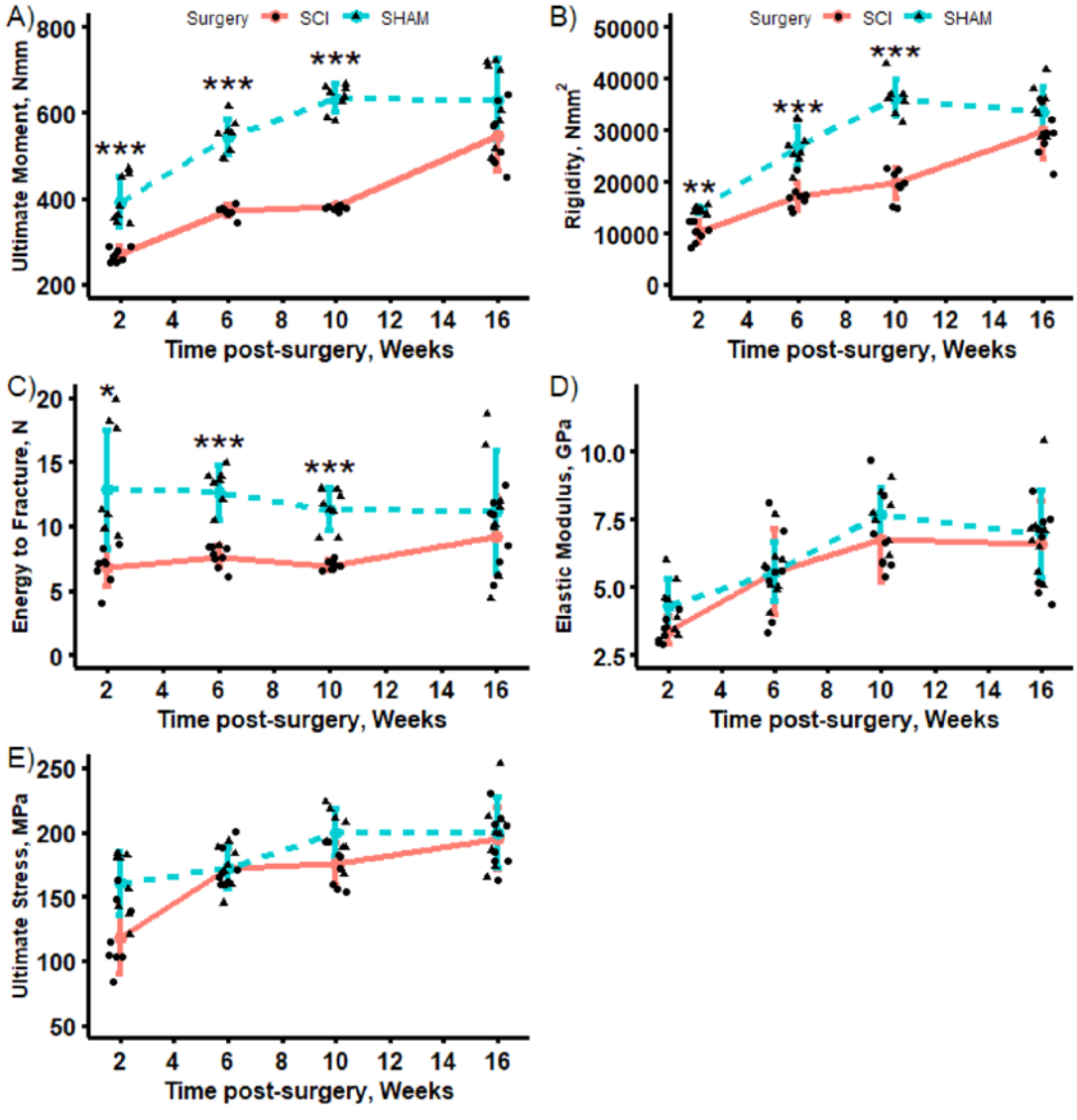

Figure 5. Three-point bend-determined whole-bone and material-level mechanical properties for 2-, 6-, 10- and 16-weeks post-surgery SCI and SHAM groups (all n=8). Whole-bone mechanical properties were adjusted for body mass using the linear regression method. Data shown as mean ± SD. *, ** and *** indicate p<0.05, p<0.01 and p<0.001, respectively, for SCI versus SHAM at the same post-surgical timepoint.

indicated that SCI exhibited lower epiphyseal BV/TV, vBMD and Tb.N and higher Tb.Sp, Tb.Pf and uPi compared to SHAM. Time main effects indicated higher BV/TV, vBMD, Tb.Th (SCI only), Tb.N, and lower Tb.Sp, BS/BV, Conn.D and uPi for later time points post-surgery in SHAM and SCI groups.

At 2-weeks post-surgery, SCI experienced 16% and 23% lower epiphyseal vBMD and BV/TV (both p<0.001), respectively, compared to SHAM. The lowering of BV/TV was characterised by 15% lower Tb.Th (p<0.001). These structural changes led to 23% higher BS/BV (p<0.001), 14% higher Tb.Pf (p<0.01) and 4% higher uPi (p<0.001). At the later time points post-surgery, SCI and SHAM epiphyseal VOIs exhibited increased vBMD and BV/TV (both p < 0.05). The 25% increase in BV/TV (p<0.001) for SHAM between 2- and 10-weeks post-surgery was characterised primarily by increased Tb.N, while 42% increase in BV/TV (p<0.001) for SCI between 2- and 16-weeks post-surgery, was due to increased Tb.Th.

µCT Analysis of Cortical Morphometry

Representative distal femoral metaphyseal and mid-diaphyseal cortical bone VOIs and morphometric measures are shown in Figures 3 and 4, respectively. Group main

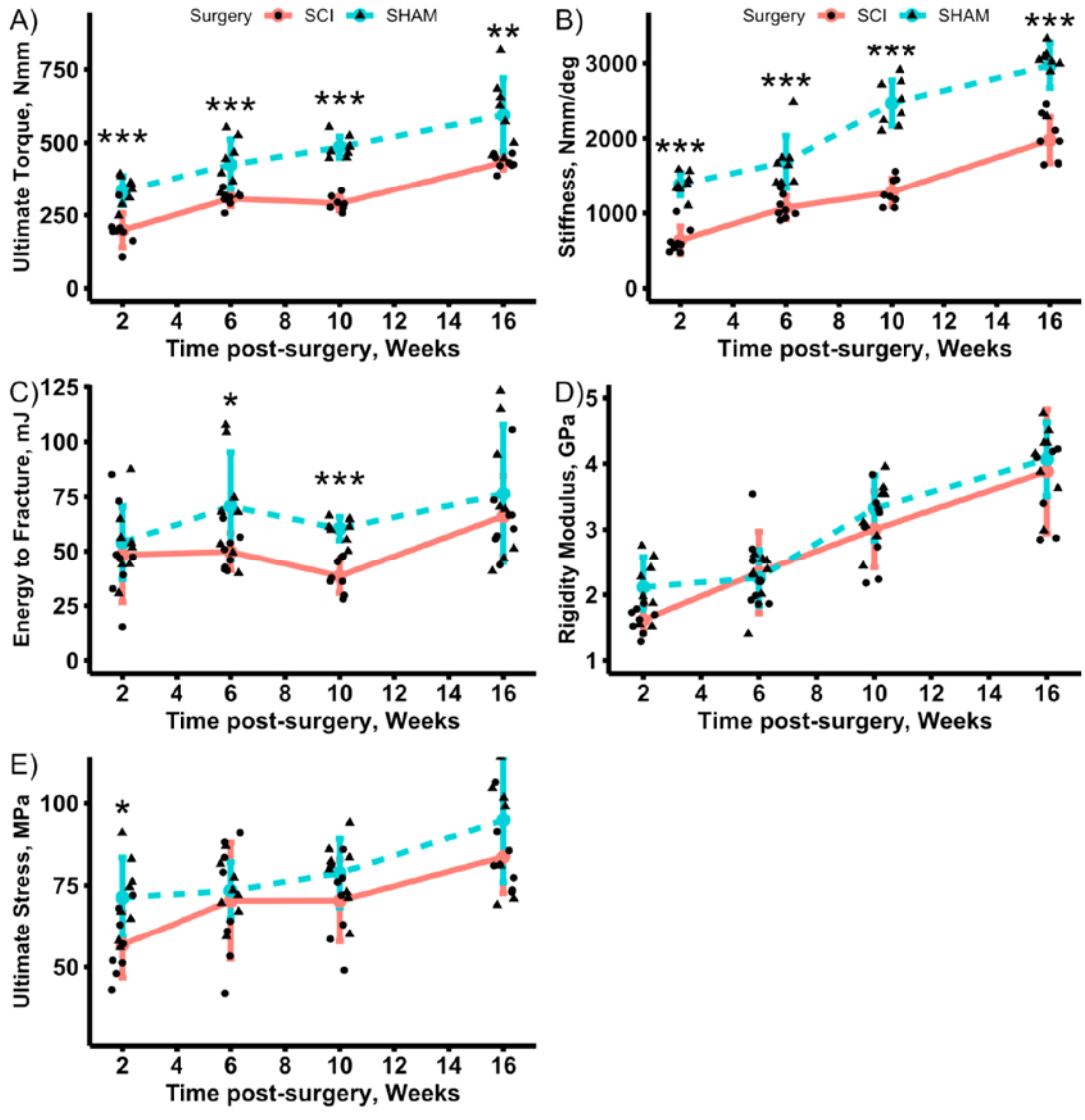

Figure 6. Torsion test-determined whole-bone and material-level mechanical properties for 2-, 6-, 10- and 16-weeks post-surgery SCI and SHAM groups (all n=8). Whole-bone mechanical properties were adjusted for body mass using the linear regression method. Data shown as mean ± SD. *, ** and *** indicate p<0.05, p<0.01 and p<0.001, respectively, for SCI versus SHAM at the same post-surgical timepoint.

effects indicate that SCI groups exhibited lower Tt.Ar, Ct.Ar, Ma.Ar, Ct.Th (mid-diaphysis only) and J, as well as higher BS/BV (mid-diaphysis only) at both cortical sites. Time main effects indicated higher Tt.Ar (SHAM only), Ct.Ar, Ct.Th (except metaphyseal SHAM), J (except metaphyseal SHAM), Ecc (SHAM only) and Ct.Ar/Tt.Ar (diaphysis only) and lower BS/BV (except metaphyseal SHAM) for later time points post-surgery in SHAM and SCI groups. This suggests a general trend of increasing cortical mass accumulation with time post-surgery for both metaphyseal and diaphyseal VOIs, in both SCI and SHAM groups, but these changes occurred at different rates. Between 2- and 10-weeks post-surgery only SHAM rats exhibited a progressive increase in Ct.Ar, Tt.Ar, Ct.Th (diaphysis only), J and Ecc. In SCI, increases in cortical structural parameters were only observed between 10- and 16-weeks.

At 2-weeks post-surgery, in both metaphyseal and diaphyseal VOIs Ct.Ar was lower, by 17% (p<0.01) and 10% (p<0.05), respectively, in SCI compared to SHAM. The metaphyseal change was characterised by 12% (p<0.01) and 10% (p<0.05) lower Tt.Ar and Ma.Ar, respectively. These structural changes contributed to 12% lower Ct.Th (p<0.01) and BS/BV (p<0.05), and 26% (p<0.01) lower J. Thereafter, Ct.Ar was only lower at 10-weeks (p<0.05), but Ma.Ar, Tt.Ar

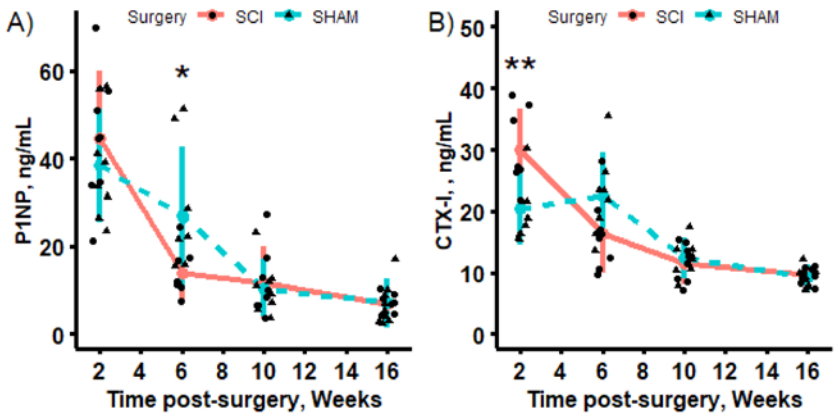

Figure 7. Serum bone turnover marker levels for 2-, 6-, 10- and 16-weeks post-surgery SCI and SHAM groups (all n=8). Data shown as mean ± SD.* and ** indicate p<0.05 and p<0.01, respectively for SCI versus SHAM at the same post-surgical timepoint. A) bone formation marker P1NP. B) bone resorption marker CTX-I.

and J remained lower (all p<0.05) in SCI for all later time point groups.

In contrast, the 2-week post-surgery diaphyseal change led to a 12% (p<0.01) and 11% (p<0.05) lowering of Ct.Th and Ct.Ar/Tt.Ar, respectively, and 13% (p<0.01) higher BS/BV in SCI compared to SHAM. Thereafter, Ct.Ar and Ct.Th remained lower, while BS/BV remained higher in SCI for all later time point groups. Tt.Ar and Ma.Ar were lower (p<0.05) at 6- and 10-weeks post-surgery, Ecc at 10- and 16-weeks post-surgery and J at all three of these later time points in SCI compared to SHAM.

Cortical Density

There was no difference in either metaphyseal or mid-diaphyseal cortical TMD between SCI and SHAM at any time point (Figures 3I and 4I). Time main effects indicated higher TMD at later post-surgical time points.

Mechanical Testing

Femoral three-point bend-derived and torsion-derived mechanical properties are shown in Figures 5 and 6, respectively. Group main effects indicated that SCI exhibited lower ultimate moment, rigidity and energy-to-fracture compared to SHAM. Time main effects indicated higher ultimate moment, rigidity, elastic modulus and ultimate tensile stress for later time points in both SCI and SHAM groups. At 2-weeks post-surgery, ultimate moment, rigidity and energy-to-fracture were 31%, 30% and 47% lower (all p<0.05), respectively, in SCI compared to SHAM. A maximum difference of 40% and 46% (both p<0.001) were observed at 10-weeks for ultimate moment and rigidity between SCI and SHAM.

Group main effects indicated that SCI exhibited lower ultimate torque and rotational stiffness compared to SHAM. Time main effects indicated higher ultimate torque, rotational stiffness, rigidity modulus and ultimate shear stress at later time points post-surgery in both SCI and SHAM groups. At 2-weeks post-surgery, ultimate torque, rotational stiffness, rigidity modulus and ultimate shear stress were 41%, 54%, 24% and 20% (all p<0.05) lower in SCI compared to SHAM, respectively. At 16-weeks post-surgery ultimate torque and rotational stiffness were 27% and 36% lower (both p<0.001), in SCI respectively.

Serum Measurements

P1NP was found to be 52% lower (p<0.05) at 6-weeks post-surgery and CTX-I was found to be 47% higher (p<0.01) at 2-weeks post-surgery in the SCI group (Figure 7).

Fourier Transform Infrared (FTIR) Spectroscopy

No significant differences were found for any average compositional parameter between 10-week post-surgery SCI and SHAM groups (Online Resource 13). With regards to heterogeneity within the samples, collagen maturity was higher in SCI compared to SHAM (p<0.05).

Discussion

SCI resulting in paralysis below the lesion triggers rapid and significant muscle atrophy and osteoporotic changes to the quantity and microstructure of bone in the affected limbs[31]. This leads to an elevated risk of fragility fractures, particularly in the trabecular-rich distal femur and proximal tibia, compared to the able-bodied population, which increases with time post-injury[2]. In this study, SCI was modelled in young skeletally immature rats (approximately 8-weeks-old) by a T9 spinal cord transection and the time

course effects on the structural and mechanical properties of the distal femur were assessed. The data suggests that: i) longitudinal bone growth was not affected by SCI; ii) there were site-specific trabecular bone changes within the distal femur post-SCI, with metaphyseal trabecular bone undergoing rapid and severe deterioration in bone quantity and microstructure, while epiphyseal trabecular bone was more structurally resistant to SCI-induced deterioration; iii) cortical bone changes were also site-specific, with metaphyseal regions experiencing the most severe lowering of Ct.Ar at 2-weeks post-injury, cortical bone changes overall were more prolonged than trabecular bone changes, with group and time main effects indicating delayed cortical bone mass accumulation and reduced spatial distribution of cortical bone in SCI relative to SHAM; iv) cortical TMD remained unaffected by SCI; v) both three-point bend- and torsion-derived cortical whole-bone mechanical properties were lowered after SCI, with no overall indication of material-level changes, and vi) the bone resorption marker CTX-I was only raised at 2-weeks post-SCI, while the bone formation marker P1NP was lowered at 6-weeks post-SCI only.

Several human SCI studies describe an exponential decline in vBMD in trabecular regions of sublesional long bones, stabilising at less than 50% of pre-injury values, between 4-and 7-years after injury[32,33]. Our study shows rapid trabecular bone changes within the metaphysis, characterised by 58% lower trabecular vBMD, and 59% lower BV/TV with associated microstructural changes (lower Tb.N, Tb.Th and Conn.D, and higher Tb.Sp, BS/BV, Tb.Pf and uPi) within 2-weeks of SCI. uPi is an alternative to the structural model index, as it increases it indicates that overall the trabecular bone VOI departs from the structurally stronger plate-like to a rod-like configuration, characterised by thinner, elongated trabeculae[21]. It is noted that at 2-weeks post-surgery circulating CTX-I was elevated, while P1NP was comparable to SHAM. At the later time points post-surgery, there were no further changes in BV/TV for either SHAM or SCI. Despite this, at the later time points microstructural changes occurred, overall there were similar trends between SHAM and SCI at these later time points, such as trabecular thickening and loss of connectivity. These results suggest that acute osteoclastic resorptive activity is increased which appears to be transient in these young rats, reducing with time post-surgery. These results are in accordance with Minematsu et al. (2014)[9], where after low thoracic transection in young male rats, a similarly severe proximal tibial metaphyseal trabecular lowering was observed after the first week, while further microstructural changes were rarely observed in 3- and 5-week groups. Also, Morse et al. (2008)[6] observed increased osteoclastic activity at 10-days post-SCI in 7-week-old T10 contusion injured rats. Contrary to our results, Jiang et al. (2007a)[5] observed elevated circulating bone resorption marker NTX at 3- and 6-weeks, and 6-months post-SCI in 6-week-old male rats. Our results are suggestive of a new steady-state being reached with lower trabecular bone mass, on a background of continued bone growth, very early on after SCI. These results are also in accordance with all previous young rat SCI-induced osteoporosis studies, where over 1- to 16-weeks post-SCI, a 37 to 73% lowering of metaphyseal BV/TV is observed[4–9,12,13]. No trend between time post-SCI and lowering of BV/TV is apparent across these studies. Interestingly, rapid and marked trabecular microstructural changes have been observed in skeletally mature rats that received incomplete contusion SCI[16]. 2-weeks post-SCI distal femoral metaphyseal trabecular BV/TV was over 50% lower than time-matched SHAM, characterised by lower Tb.N and Tb.Th[16]. However, no time course studies of transection SCI-induced osteoporosis in skeletally mature have been performed.

Epiphyseal sites at the ends of long bones are by far the most commonly assessed site in human SCI pQCT studies and only Dudley-Javoroski and Shields (2012)[34] have quantified changes in the metaphysis. Despite this, only one previous rat SCI-induced osteoporosis study has examined the epiphysis[11]. In our study, epiphyseal trabecular bone also underwent a rapid lowering of vBMD and BV/TV, but less marked than within the metaphysis. The epiphyseal BV/TV change was characterised by lower average Tb.Th, indicating that trabeculae that were originally thicker than those in the metaphysis thinned but were not removed entirely. Thus, the connectivity of the epiphyseal compartment remained intact after SCI. This result is in accordance with Lin et al. (2015)[11], who in 4-month-old male rats with a T9-contusion SCI, examined 16-weeks post-injury, observed a much milder deterioration of epiphyseal compared to metaphyseal trabecular bone. A second difference between epiphyseal and metaphyseal trabecular bone observed in our study was that epiphyseal vBMD and BV/TV increased between 2- and 16-weeks for SCI and SHAM as the femurs continued to grow, indicating a net gain in both trabecular BV and BV/TV. Thus, there were site-specific and time-specific differences in the structural effects of SCI on both compartments. This time course change in the epiphyseal compartment has not been observed in children with SCI, in fact a continued reduction in epiphyseal vBMD was observed between serial pQCT from an initial scan at an average of 7.6 years and follow-up scan 10.7 years post-SCI[35].

Adult humans with SCI experience cortical bone loss through endocortical thinning (marrow expansion), before new geometric and densiometric steady-states are eventually reached, typically a number of years post-SCI[32,33]. These cortical bone changes occur more slowly than trabecular changes[32]. A rapid and marked site-specific cortical response was found in our study. At 2-weeks post-SCI metaphyseal cortical bone was more severely affected than diaphyseal bone in terms of reduction in Ct.Ar compared to SHAM. This difference was at least in part due to the metaphysis having a significantly higher BS/BV than the diaphysis, which equates to a larger surface area on which bone turnover can occur on. This result is in accordance with human SCI-induced osteoporosis, where more pronounced changes are observed distally compared to the shaft of a long bone[36]. In our young rat model, Tt.Ar for metaphyseal cortical bone

was lower from 2-weeks and for mid-diaphyseal cortical bone was lower between 6- and 10-weeks post-surgery in SCI. This suggests diminished periosteal expansion, resulting in reduced periosteal bone apposition throughout the distal femur. The smaller Tt.Ar and Ct.Ar led a decrease in J, the geometric parameter related to torsional strength and stiffness. The torsional failure site was consistently supracondylar, occurring within the metaphysis and torsional testing suggested that lower J led to proportionally weak bone. For the diaphysis, significant cortical thinning was observed in SCI at all time points, but not through endocortical thinning (marrow expansion) and eccentricity, which is a geometric parameter responsive to load bearing[37], was decreased from 10-weeks in SCI compared to SHAM. These result are consistent with what is observed in the long bones of children with SCI, where Ct.Ar, Tt.Ar and eccentricity of the diaphysis are reduced when compared with controls[35]. For the SHAM groups, metaphyseal Ct.Th remained relatively constant with time post-surgery, this appears a consequence of the longitudinal growth process, and is in accordance with clinical observations seen in young children[38]. Despite a persistent lowering of Tt.Ar, Ma.Ar and J after SCI, there was only an initial cortical thinning in the 2-week SCI group. At later time points Ct.Th was comparable for SCI and SHAM, but the spatial distribution of cortical bone in SCI was always significantly reduced. This suggests that SCI-induced cortical bone changes are a combination of bone loss and supressed bone apposition. Interestingly, in skeletally mature contusion SCI rats Otzel et al. (2019)[16] did not observe a lowering of Tt.Ar at the mid-diaphysis. Although there was evidence for lower Tt.Ar at more distal cortical sites in SCI, compared to age-matched SHAMs, but their difference versus SHAM was considerably less marked than that observed in our study.

Metaphyseal and diaphyseal cortical TMD did not significantly differ between any age-matched SCI and SHAM groups, which is in accordance with Lin et al. (2015)[11]. Whole-bone mechanical properties (both three-point bend- and torsion-derived) were overall lower in SCI which is in accordance with Beggs et al. (2015)[10], Jiang et al. (2006b)[4] and Liu et al. (2008a)[7], while tissue-level properties were similar between SCI and SHAM, which is in accordance with Sugawara et al. (1998)[39]. These results suggest that the reduction in femoral strength is not due to changes in bone material properties, but due to changes in the spatial distribution of the bone material. Whole-bone mechanical properties derived from three-point bend and torsion testing were normalised for body mass, the results suggested that bone strength and stiffness in SCI rats were not appropriate for body size, but significantly lower.

The cross-sectional experimental design as opposed to a truly longitudinal design can be a limitation. Using *in vivo* µCT to follow up the same rats at different time points, would allow microstructural changes in the same bone to be observed. However, this would not have allowed mechanical testing at each time point. To our knowledge, only one rodent study has used *in vivo* µCT to examine SCI-induced osteoporosis, where only proximal tibia metaphyseal BV/TV was monitored at 0-, 2- and 8-weeks post-surgery[13]. Additionally, dynamic histomorphometry for the measure of bone formation parameters would have be a useful additional tool for investigating the mechanisms involved in the reduced cortical bone mass accumulation and spatial distribution observed here.

To conclude, this model resembles the rapid metaphyseal trabecular bone changes observed clinically in both adults and juveniles with SCI. It is therefore a suitable model for testing the efficacy of therapeutic interventions aimed at preventing, attenuating or reversing SCI-induced osteoporosis. This study also highlights that caution must be exercised when interpreting results from young rat studies. The young rat model used in this study overall mimics better the cortical bone changes observed following SCI in children and young adults, where bone changes cannot be solely attributed to bone loss, but also suppressed bone apposition, which is a different mechanism from the SCI-induced bone loss observed in adults. This indicates that optimised models should be considered, depending on the mechanisms of interest, younger rats may better represent bone changes in paediatric SCI in particular, while older, skeletally mature rat models may better represent adult SCI.

Funding

This study was supported by funding from the Engineering and Physical Sciences Research Council (EPSRC) Life Sciences Interface Programme (EP/F50036X/1) and in part by the European Research Council under the European Union's Seventh Framework Programme (FP/2007-2013)/ERC Grant Agreement no. 615030. Carmen Huesa was supported by the Versus Arthritis early career fellowship (grant no. 22483). Data collected in this study is accessible at https://doi.org/10.15129/e345cd3a-e306-4ceb-b1c3-616da9ec40bd.

Acknowledgements

We thank Diamond Light Source for access to the MIRIAM beamline, B22, (proposal 15102) and assistance from beamline scientist Chris Kelly.

References

1. Jiang S-D, Dai L-Y, Jiang L-S. Osteoporosis after spinal cord injury. Osteoporos Int 2006;17(2):180–92.
2. Dauty M, Perrouin Verbe B, Maugars Y, Dubois C, Mathe JF. Supralesional and sublesional bone mineral density in spinal cord-injured patients. Bone 2000; 27(2):305–9.
3. Zehnder Y, Lüthi M, Dieter M, Knecht H, Perrelet R, Neto I, Kraenzlin M, Zach G, Lippuner K. Long-term changes in bone metabolism, bone mineral density, quantitative ultrasound parameters, and fracture incidence after spinal cord injury: a cross-sectional observational study in 100 paraplegic men. Osteoporos Int 2004; 15(3):180–9.
4. Jiang S-D, Jiang L-S, Dai L-Y. Spinal cord injury causes more damage to bone mass, bone structure, biomechanical properties and bone metabolism than sciatic neurectomy in young rats. Osteoporos Int

2006;17(10):1552–61.
5. Jiang S, Jiang L, Dai L. Changes in Bone Mass, Bone Structure, Bone Biomechanical Properties, and Bone Metabolism after Spinal Cord Injury: A 6-Month Longitudinal Study in Growing Rats. Calcif Tissue Int 2007;80;167-75.
6. Morse L, Teng YD, Pham L, Newton K, Yu D, Liao WL, Kohler T, Müller R, Graves D, Stashenko P, Battaglino R. Spinal cord injury causes rapid osteoclastic resorption and growth plate abnormalities in growing rats (SCI-induced bone loss in growing rats). Osteoporos Int 2008;19(5):645–52.
7. Liu D, Li H, Zhao CQ, Jiang LS, Dai LY. Changes of substance P-immunoreactive nerve fiber innervation density in the sublesional bones in young growing rats at an early stage after spinal cord injury. Osteoporos. Int. 2008;19(4):559–69.
8. Liu D, Zhao C-Q, Li H, Jiang S-D, Jiang L-S, Dai L-Y. Effects of spinal cord injury and hindlimb immobilization on sublesional and supralesional bones in young growing rats. Bone 2008;43(1):119–25.
9. Minematsu A, Nishii Y, Imagita H, Sakata S. Time Course of Changes in Trabecular Bone Microstructure in Rats with Spinal Cord Injury. J Life Sci 2014;8(6):522–8.
10. Beggs LA, Ye F, Ghosh P, Beck DT, Conover CF, Balaez A, Miller JR, Phillips EG, Zheng N, Williams AA, Aguirre J, Wronski TJ, Bose PK, Borst SE, Yarrow JF. Sclerostin inhibition prevents spinal cord injury-induced cancellous bone loss. J Bone Miner Res 2015;30(4):681–9.
11. Lin T, Tong W, Chandra A, Hsu S-Y, Jia H, Zhu J, Tseng W-J, Levine MA, Zhang Y, Yan S-G, Liu XS, Sun D, Young W, Qin L. A comprehensive study of long-term skeletal changes after spinal cord injury in adult rats. Bone Res 2015;3:1–9.
12. Jiang S-D, Shen C, Jiang L-S, Dai L-Y. Differences of bone mass and bone structure in osteopenic rat models caused by spinal cord injury and ovariectomy. Osteoporos Int 2007;18(6):743–50.
13. Voor MJ, Brown EH, Xu Q, Waddell SW, Burden RL, Burke DA, Magnuson DSK. Bone loss following spinal cord injury in a rat model. J Neurotrauma 2012; 29(8):1676–82.
14. Parent S, Mac-Thiong J-M, Roy-Beaudry M, Sosa JF, Labelle H. Spinal Cord Injury in the Pediatric Population: A Systematic Review of the Literature. J Neurotrauma 2011;28(8):1515–24.
15. Yarrow JF, Ye F, Balaez A, Mantione JM, Otzel DM, Chen C, Beggs LA, Baligand C, Keener JE, Lim W, Vohra RS, Batra A, Borst SE, Bose PK, Thompson FJ, Vandenborne K. Bone loss in a new rodent model combining spinal cord injury and cast immobilization 2014;14(255):255–66.
16. Otzel DM, Conover CF, Ye F, Phillips EG, Bassett T, Wnek RD, Flores M, Catter A, Ghosh P, Balaez A, Petusevsky J, Chen C, Gao Y, Zhang Y, Jiron JM, Bose PK, Borst SE, Wronski TJ, Aguirre JI, Yarrow JF. Longitudinal Examination of Bone Loss in Male Rats After Moderate–Severe Contusion Spinal Cord Injury. Calcif Tissue Int 2019;104(1):79–91.
17. Peng Y, Zhao W, Hu Y, Li F, Guo XE, Wang D, Bauman WA, Qin W. Rapid bone loss occurs as early as 2 days after complete spinal cord transection in young adult rats. Spinal Cord 2020;58(3):309–17.
18. Williams JA, Windmill JFC, Tanner KE, Riddell JS, Coupaud S. Global and site-specific analysis of bone in a rat model of spinal cord injury-induced osteoporosis. Bone Reports 2019;12:100233.
19. Bouxsein ML, Boyd SK, Christiansen BA, Guldberg RE, Jepsen KJ, Müller R. Guidelines for assessment of bone microstructure in rodents using micro-computed tomography. J Bone Miner Res 2010;25(7):1468–86.
20. Hahn M, Vogel M, Pompesius-Kempa M, Delling G. Trabecular bone pattern factor - A new parameter for simple quantification of bone microarchitecture. Bone 1992;13(4):327–30.
21. Salmon P. Application of Bone Morphometry and Densitometry by X-Ray Micro-CT to Bone Disease Models and Phenotypes. Micro-computed Tomogr. Med. Eng. Cham: Springer; 2020.
22. Bruker. Morphometric parameters measured by Skyscan TM CT - analyser software . [Internet]. Available from: http://bruker-microct.com/next/CTAn03.pdf
23. Jepsen KJ, Silva MJ, Vashishth D, Guo XE, van der Meulen MCH. Establishing biomechanical mechanisms in mouse models: Practical guidelines for systematically evaluating phenotypic changes in the diaphyses of long bones. J Bone Miner Res 2015;30(6):951–66.
24. Turner C, Burr D. Basic biomechanical measurements of bone: a tutorial. Bone 1993;14(4):595–608.
25. Bosemark P, Isaksson H, Tägil M. Influence of systemic bisphosphonate treatment on mechanical properties of BMP-induced calluses in a rat fracture model: Comparison of three-point bending and twisting test. J Orthop Res 2014;(May):721–6.
26. Boskey A, Camacho NP. FT-IR imaging of native and tissue-engineered bone and cartilage. Biomaterials 2007;28(15):2465-78
27. Spevak L, Flach CR, Hunter T, Mendelsohn R, Boskey A. Fourier transform infrared spectroscopic imaging parameters describing acid phosphate substitution in biologic hydroxyapatite. Calcif Tissue Int 2013; 92(5):418–28.
28. Paschalis EP, Verdelis K, Doty SB, Boskey AL, Mendelsohn R, Yamauchi M. Spectroscopic characterization of collagen cross-links in bone. J Bone Miner Res 2001;16(10):1821–8.
29. Isaksson H, Turunen MJ, Rieppo L, Saarakkala S, Tamminen IS, Rieppo J, Kröger H, Jurvelin JS. Infrared spectroscopy indicates altered bone turnover and remodeling activity in renal osteodystrophy. J Bone Miner Res 2010;25(6):1360–6.
30. Boskey AL, Spevak L, Weinstein RS. Spectroscopic markers of bone quality in alendronate-treated postmenopausal women. Osteoporos Int 2009; 20(5):793–800.

31. Cirnigliaro CM, Myslinski MJ, La Fountaine MF, Kirshblum SC, Forrest GF, Bauman WA. Bone loss at the distal femur and proximal tibia in persons with spinal cord injury: imaging approaches, risk of fracture, and potential treatment options. Osteoporos Int 2017;28(3):747–65.
32. Eser P, Frotzler A, Zehnder Y, Wick L, Knecht H, Denoth J, Schiessl H. Relationship between the duration of paralysis and bone structure: a pQCT study of spinal cord injured individuals. Bone 2004;34(5):869–80.
33. Frotzler A, Berger M, Knecht H, Eser P. Bone steady-state is established at reduced bone strength after spinal cord injury: A longitudinal study using peripheral quantitative computed tomography (pQCT). Bone 2008;43(3):549–55.
34. Dudley-Javoroski S, Shields RK. Regional cortical and trabecular bone loss after spinal cord injury. J Rehabil Res Dev 2012;49(9):1365–76.
35. Biggin A, Briody JN, Ramjan KA, Middleton A, Waugh MCA, Munns CF. Evaluation of bone mineral density and morphology using pQCT in children after spinal cord injury. Dev Neurorehabil 2013;16(6):391–7.
36. Rittweger J, Goosey-Tolfrey VL, Cointry G, Ferretti JL. Structural analysis of the human tibia in men with spinal cord injury by tomographic (pQCT) serial scans. Bone 2010;47(3):511–8.
37. Marenzana M, Souza RL De, Chenu C. Blockade of beta-adrenergic signaling does not influence the bone mechano-adaptive response in mice. Bone 2007;41:206–15.
38. Rauch F, Schönau E. Peripheral quantitative computed tomography of the distal radius in young subjects – new reference data and interpretation of results. J. Musculoskelet. Neuronal Interact 2005;5(2):119–26.
39. Sugawara H, Linsenmeyer TA, Beam H, Parsons JR. Mechanical properties of bone in a paraplegic rat model. J Spinal Cord Med 1998;21(4):302–8.

Supplemental Material

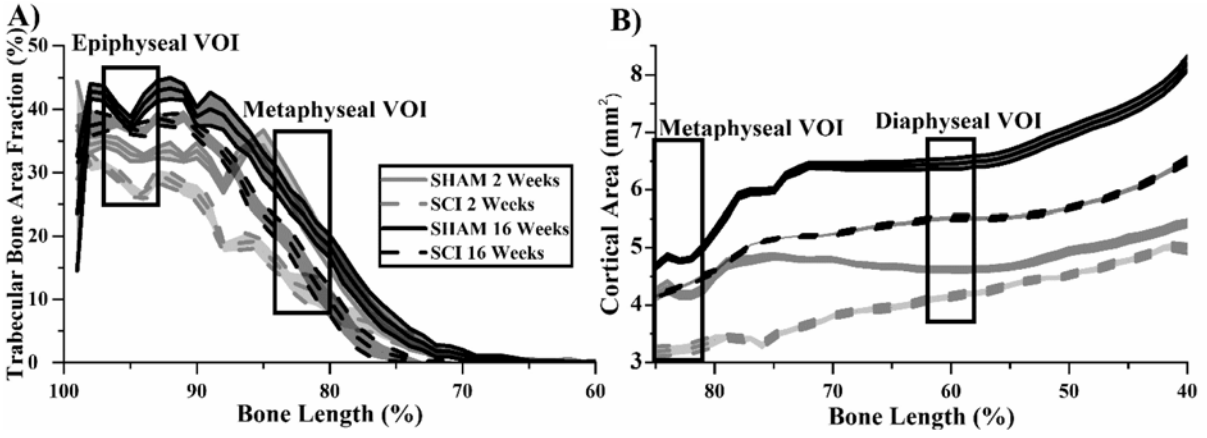

Online Resource 1. Global 2D morphometric analysis of A) trabecular bone area fraction for 60 to 100% bone length and B) cortical area for 40 to 85% bone length for 2- and 16-week post-surgery SCI and SHAM rats. Trabecular and cortical VOIs used for subsequent 3D are superimposed on distributions. Data shown as mean ± SE for every 1% bone length.

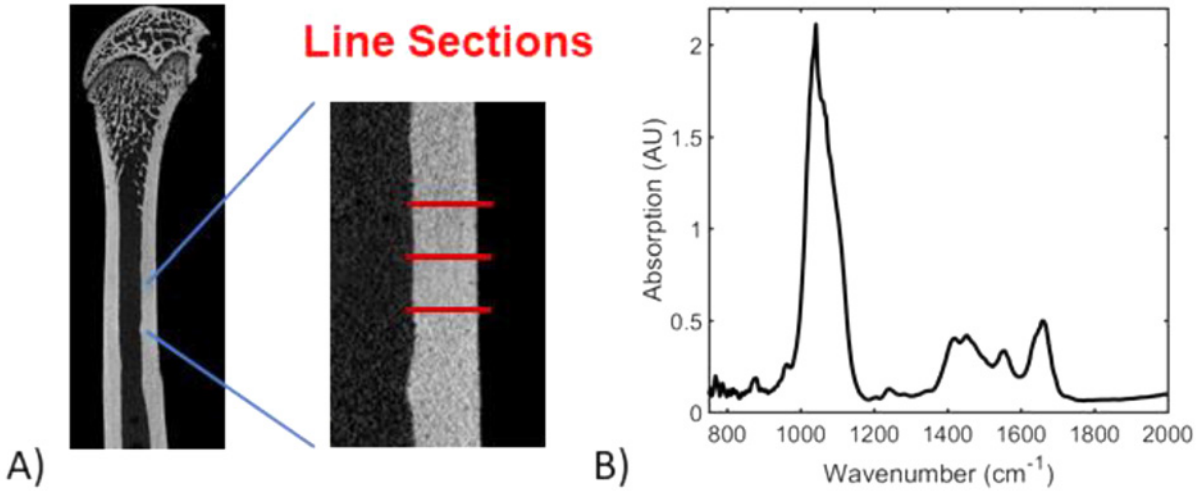

Online Resource 2. Schematics to represent location, measurement approach and collected FTIR spectra.

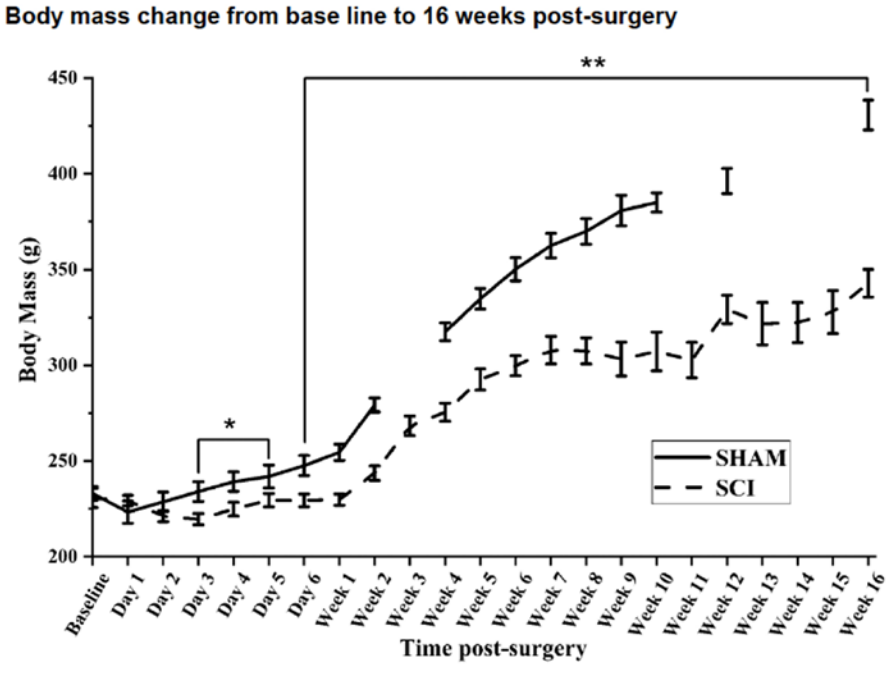

Online Resource 3. Body mass with time post-surgery for SCI and SHAM rats. Data shown as mean ± SE. * and ** indicate $p < 0.05$ and $p < 0.01$, respectively, for SCI versus SHAM at the same post-surgical timepoint.

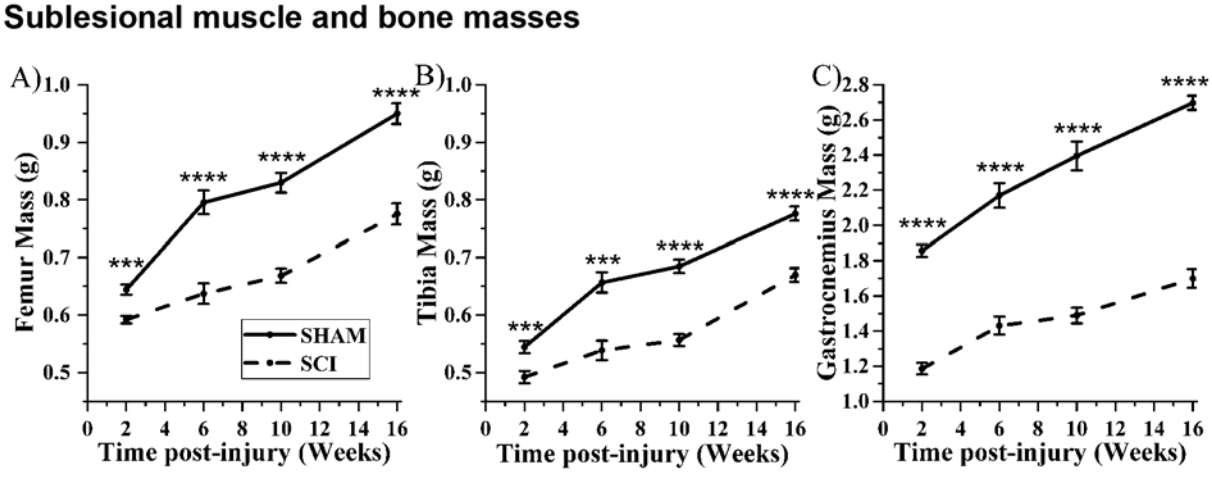

Online Resource 4. Sublesional bone wet masses and muscle mass for SCI and SHAM rats at 2-, 6-, 10- and 16-weeks post-surgery for the right hindlimb. A) Femur wet mass, B) Tibia wet mass and C) gastrocnemius (both medial and lateral heads) muscle mass. Data shown as mean ± SE. *** and **** indicate $p < 0.001$ and $p<0.0001$, respectively, for SCI versus SHAM at the same post-surgical timepoint.

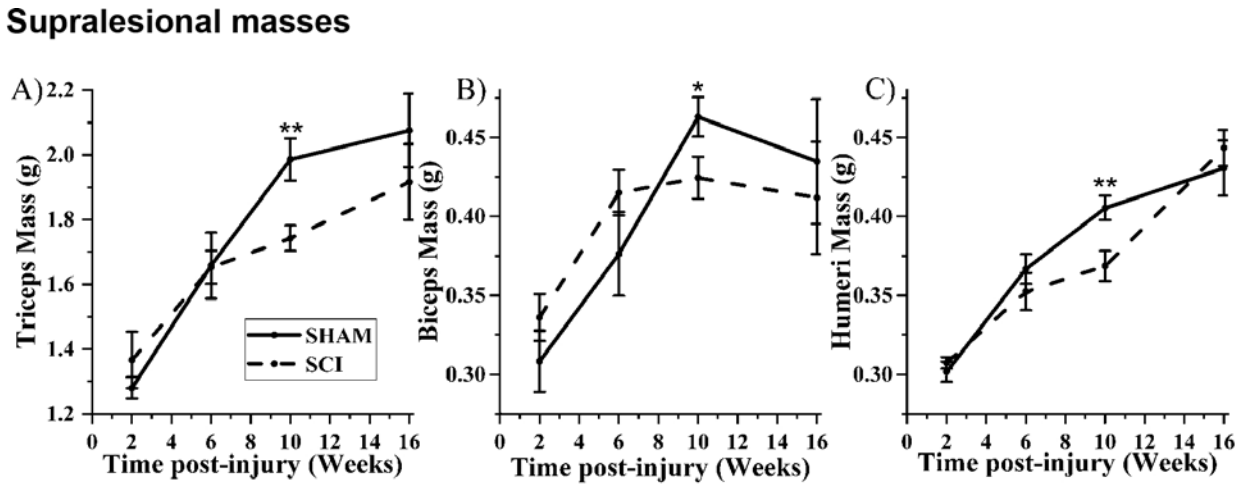

Online Resource 5. Supralesional bone wet mass and muscle masses for SCI and SHAM rats at 2-, 6-, 10- and 16-weeks post-surgery for the right forelimb. A) Tricep mass, B) Bicep mass and C) Humeri wet mass. Data shown as mean ± SE. * and ** indicate p<0.05 and p<0.01, respectively, for SCI versus SHAM at the same post-surgical timepoint.

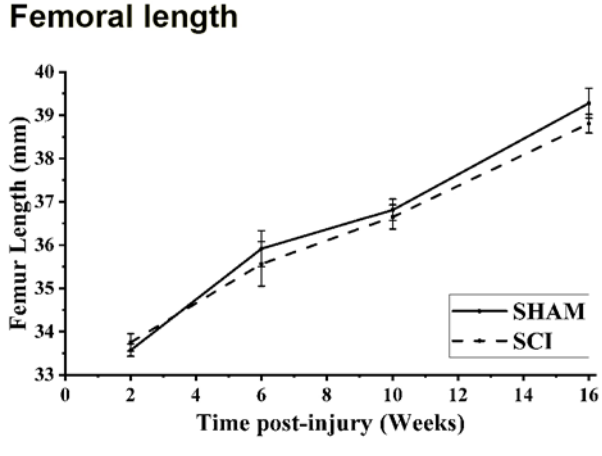

Online Resource 6. Femoral length for SCI and SHAM rats at 2-, 6-, 10- and 16-weeks post-surgery. Data shown as mean ± SE.

Online Resource 7. 3D distal femoral metaphyseal secondary spongiosa (81 – 85% bone length) average morphology for SHAM and SCI rats at 2-, 6-, 10- and 16-weeks post-surgery.

	SHAM				SCI			
	2 Weeks (n = 8)	6 Weeks (n = 8)	10 Weeks (n = 8)	16 Weeks (n = 9)	2 Weeks (n = 8)	6 Weeks (n = 8)	10 Weeks (n = 8)	16 Weeks (n = 8)
BV (mm^3)	4.86 ± 0.63 (3.33 –6.39)	6.67 ± 0.52[a] (5.43 – 7.90)	6.24 ± 0.42 (5.24 – 7.23)	6.28 ± 0.68 (4.61 – 7.95)	2.20 ± 0.45* (1.03 – 3.36)	1.70[*,a] ±0.21* (1.19 – 2.21)	1.91 ± 0.49* (0.65 – 3.17)	2.86 ± 0.24[*,b] (2.26 – 3.45)
$BV/TV^{S,S-T}$ (%)	23.41 ± 2.53 (17.22 – 29.59)	25.45 ± 1.67 (21.50 – 29.41)	26.29 ± 1.43 (22.91 – 29.67)	24.20 ± 2.26 (18.68 – 29.72)	9.55 ± 1.81* (4.91 – 14.20)	8.76 ± 1.16* (6.02 – 11.50)	9.04 ± 1.88* (4.22 – 13.86)	12.35 ± 0.80* (10.39 – 14.31)
BS/BV (mm^{-1})	48.43 ± 1.94 (43.69 – 53.17)	46.75 ± 1.98 (42.07 – 51.43)	43.07± 1.88[a,b] (39.10 – 47.04)	38.73± 0.74[a,b] (36.92 – 40.55)	63.02± 3.24* (54.69 – 71.35)	55.75± 1.23*[,a] (52.84 – 58.64)	53.35± 1.85*[,a] (48.58 – 58.12)	43.46±1.23*[,a,b] (40.44 – 46.48)
$Tb.Th^{S,T,S-T}$ (mm)	0.08 ± 0.00 (0.07 – 0.08)	0.08 ± 0.00 (0.07 – 0.08)	0.08 ± 0.00[a,b] (0.08 – 0.09)	0.09 ±0.00[a,b,c] (0.09 – 0.10)	0.06 ± 0.00* (0.06 – 0.07)	0.07 ± 0.00 (0.07 – 0.07)	0.07 ± 0.00*[,a] (0.07 – 0.08)	0.09 ± 0.00[a,b,c] (0.08 – 0.10)
$Tb.Sp^{S,S-T}$ (mm)	0.31 ± 0.04 (0.21 – 0.41)	0.29 ± 0.03 (0.23 – 0.36)	0.26 ± 0.02 (0.21 - 0.32)	0.34 ± 0.03 (0.27 – 0.42)	0.51 ± 0.07* (0.33 – 0.70)	0.69 ± 0.09* (0.48 – 0.91)	0.81 ± 0.14* (0.44 – 1.16)	0.52 ± 0.04* (0.42 – 0.61)
$Tb.N^{S,S-T}$ (mm^{-1})	3.10 ± 0.27 (2.49 –3.75)	3.35 ± 0.20 (2.87 – 3.83)	3.10 ± 0.15 (2.75 – 3.46)	2.57 ± 0.24 (1.98 – 3.16)	1.47 ± 0.24* (0.85 – 2.08)	1.22 ± 0.15* (0.87 – 1.57)	1.20 ± 0.24* (0.59 – 1.82)	1.39 ± 0.08* (1.20 – 1.58)
$Tb.Pf^{S,T,S-T}$ (mm^{-1})	8.54 ± 1.22 (5.56 – 11.51)	4.15 ± 0.95[a] (1.91 – 6.39)	6.71 ± 1.23 (3.79 – 9.62)	9.19 ± 1.04[b] (6.65 – 11.73)	20.95 ± 2.03* (15.73 – 26.16)	17.28 ± 1.28* (14.25 – 30.31)	16.48 ± 1.44* (12.78 – 20.19)	15.11 ± 1.39* (11.70 – 18.51)
$uPi^{S,S-T}$	2.13 ± 0.02 (2.08 –2.19)	2.09 ± 0.02 (2.04 -2.14)	2.17 ± 0.06 (2.03 – 2.31)	2.19 ± 0.04 (2.09 – 2.29)	2.34 ± 0.04* (2.25 – 2.43)	2.35 ± 0.01* (2.32 – 2.38)	2.38 ± 0.04* (2.28 – 2.48)	2.30 ± 0.01* (2.26 – 2.33)
$Conn.D^{S,T,S-T}$ (mm^{-3})	230.5 ± 20.2 (181.2 – 279.9)	251.8 ± 28.1 (185.4 – 318.2)	229.3 ± 35.7 (144.9 – 313.8)	158.8 ± 18.2 (114.2 – 203.4)	157.0 ± 12.8* (124.2 – 189.8)	112.4 ± 15.9* (74.8 – 150.1)	94.0 ± 17.3*[,a] (49.6 – 138.5)	92.8 ± 4.7*[,a] (81.3 – 104.4)

Data presented as mean ± standard error of the mean, data in brackets represents the lower and higher bounds of the 95% confidence interval.
[S] Significant effect of SCI, [T] significant effect of time post-surgery, [S-T] significant injury-time post injury interaction; ANOVA p<0.05.
** SCI different from SHAM at same timepoint post-surgery; p<0.05.*
[a] Different from 2 weeks, [b] different from 6 weeks, [c] different from 10 weeks post-surgery; p<0.05.

Online Resource 8. 3D distal femoral epiphyseal secondary spongiosa (93 – 97% bone length) morphology for SHAM and SCI rats at 2-, 6-, 10- and 16-weeks post-surgery.

	SHAM				SCI			
	2 Weeks (n = 8)	6 Weeks (n = 8)	10 Weeks (n = 8)	16 Weeks (n = 9)	2 Weeks (n = 8)	6 Weeks (n = 8)	10 Weeks (n = 8)	16 Weeks (n = 8)
BV (mm)	11.69 ± 0.69 (9.99-13.40)	12.92 ± 0.50 (11.75-14.10)	12.96 ± 0.35 (12.12 -13.80)	11.30 ± 0.69 (9.66 – 12.94)	9.15 ± 0.55* (7.74-10.56)	11.84 ± 0.36[a] (10.99-12.70)	11.72±0.30*,[a] (10.94-12.50)	12.16 ± 0.44[a] (9.66-12.94)
BV/TV$^{S,T,S-T}$ (%)	37.11 ± 0.76 (35.26 - 38.95)	42.71a ± 0.93 (40.51 – 44.90)	46.33 ±0.69[a,b] (44.67 – 47.97)	44.24 ± 0.97[a] (41.94 - 46.54)	28.72 ± 1.73* (24.27 – 33.18)	36.79 ± 0.66*,[a] (35.24 – 38.34)	36.49±1.19*,[a] (33.44 – 39.55)	40.93±0.82*,[a,b,c] (38.99 – 42.88)
BS/BV (mm^{-1})	32.42 ± 0.51 (31.18 – 33.67)	33.53 ± 1.74 (29.41 – 37.64)	29.04 ± 0.72[b] (27.35 – 30.74)	29.39 ± 0.35[b] (28.55 – 30.23)	39.90 ± 1.00* (37.32 – 42.47)	32.20 ± 0.64[a] (30.69 – 33.70)	31.38a±0.60*,[a] (29.84 – 32.92)	29.39 ± 0.80[a,b] (28.55 – 30.23)
Tb.Th^{S,T,S_T} (mm)	0.10 ± 0.00 (0.10 – 0.11)	0.09 ± 0.00 (0.08 – 0.10)	0.11 ± 0.00[b] (0.10 – 0.11)	0.10 ± 0.00[b] (0.10 – 0.11)	0.09 ± 0.00* (0.08 – 0.09)	0.10 ± 0.00[a] (0.10 – 0.10)	0.10 ± 0.00[a] (0.10 – 0.11)	0.11 ± 0.00[a,b,c] (0.10 – 0.11)
Tb.Sp$^{S,T,S-T}$ (mm)	0.25 ± 0.01 (0.22 – 0.27)	0.20 ± 0.01 (0.18 – 0.22)	0.19 ± 0.02[a] (0.16 – 0.23)	0.20 ± 0.01 (0.18 – 0.23)	0.27 ± 0.01 (0.23 – 0.31)	0.24 ± 0.01* (0.22 – 0.26)	0.27 ± 0.01* (0.24 – 0.29)	0.22 ± 0.01[a,c] (0.20 – 0.23)
Tb.N$^{S,T,S-T}$ (mm^{-1})	3.69 ± 0.09 (3.48 – 3.90)	4.80 ± 0.18[a] (4.39 – 5.22)	4.44 ± 0.17[a] (4.03 – 4.65)	4.34 ± 0.13[a] (4.03 – 4.65)	3.36 ± 0.16 (2.96 – 3.76)	3.70 ± 0.08* (3.51 – 3.89)	3.65 ± 0.12* (3.33 – 3.97)	3.81 ± 0.08*,[a] (3.61 – 4.01)
Tb.Pf$^{S,T,S-T}$ (mm^{-1})	-2.29 ± 0.41 (-3.28 – -1.30)	-14.79 ±3.17[a] (-22.29 - 7.30)	-7.35 ± 4.05 (- 16.97 – 2.27)	-8.95 ± 1.67 (-12.89 – -5.00)	0.93 ± 0.86* (-1.28 – 3.13)	-3.01 ± 0.55* (-4.30 – -1.71)	-6.62 ± 1.81[a] (-11.27 – -1.98)	-4.28 ± 1.21*,[b] (-7.14 – -1.43)
uPi$^{S,T,S-T}$	2.00 ± 0.01 (1.98 – 2.01)	1.82 ± 0.02 (1.77 – 1.86)	1.87 ± 0.06 (1.71 – 2.02)	1.83 ± 0.02 (1.78 – 1.87)	2.07 ± 0.02* (2.04 – 2.11)	1.96 ± 0.01[a] (1.93 – 1.98)	1.92 ± 0.02[a,b] (1.86 – 1.98)	1.89 ± 0.02[a,b] (1.85 – 1.94)
Conn.D$^{T,S-T}$ (mm^{-3})	135.4 ± 7.1 (117.9 – 152.9)	126.82 ± 23.16 (72.1 – 181.6)	101.41 ± 25.31[a] (41.6 – 161.3)	78.83 ± 10.22[a] (54.7 – 103.0)	146.77±13.19 (112.9 – 180.7)	105.48 ± 9.15 (83.9 – 127.1)	84.67 ± 15.23[a] (45.5 – 123.8)	65.77 ± 6.76[a] (49.8 – 81.8)

Data presented as mean ± standard error of the mean, data in brackets represents the lower and higher bounds of the 95% confidence interval.
[S] Significant effect of SCI, [T] significant effect of time post-surgery, [S-T] significant injury-time post injury interaction; ANOVA p<0.05.
** SCI different from SHAM at same timepoint post-surgery; p<0.05.*
[a] Different from 2 weeks, [b] different from 6 weeks, [c] different from 10 weeks post-surgery; p<0.05.

Online Resource 9. 3D distal femoral metaphyseal (81 - 85% bone length) cortical bone morphology and densitometry for SHAM and SCI rats at 2-, 6-, 10- and 16-weeks post-surgery.

	SHAM				SCI			
	2 Weeks (n = 8)	6 Weeks (n = 8)	10 Weeks (n = 8)	16 Weeks (n = 9)	2 Weeks (n = 8)	6 Weeks (n = 8)	10 Weeks (n = 8)	16 Weeks (n = 8)
$Ct.Th^{S,S-T}$ (mm)	0.40 ± 0.01 (0.38 – 0.42)	0.38 ± 0.01 (0.37 – 0.40)	0.41 ± 0.00 (0.40 – 0.42)	0.39 ± 0.01 (0.37 – 0.42)	0.35 ± 0.01* (0.33 – 0.38)	0.39 ± 0.01 (0.36 – 0.42)	0.38 ± 0.02 (0.32 – 0.43)	0.40 ± 0.01 (0.38 – 0.42)
$Tt.Ar^{S,T,S-T}$ (mm^2)	12.89 ± 0.28 (12.21 – 13.56)	14.99 ± 0.61[a] (13.55 – 16.42)	14.23 ± 0.37 (13.25 – 15.20)	15.49 ± 0.39[a] (14.58 – 16.40)	11.33 ± 0.35* (10.35 – 12.31)	11.52 ± 0.35* (10.67 – 12.38)	10.49 ± 0.77* (8.51 – 12.46)	13.87 ± 0.44*[,a,b,c] (12.83 – 14.90)
$Ct.Ar^{S,T,S-T}$ (mm^2)	4.14 ± 0.15 (3.77 – 4.51)	4.34 ± 0.10 (4.11 – 4.57)	4.62 ± 0.09 (4.38 – 4.85)	4.77 ± 0.13[a] (4.46 – 5.09)	3.44 ± 0.12* (3.12 – 3.76)	3.94 ± 0.19 (3.48 – 4.39)	3.91 ± 0.24* (3.28 - 4.52)	4.51 ± 0.07[a] (4.34 – 4.69)
$Ma.Ar^{S,T,S-T}$ (mm^2)	8.75 ± 0.18 (8.32 – 9.18)	10.65 ± 0.57[a] (9.31 – 11.98)	9.61 ± 0.34 (8.72 – 10.50)	10.72 ± 0.39[a] (9.79 – 11.65)	7.88 ± 0.31* (7.01 – 8.76)	7.59 ± 0.22* (7.05 – 8.12)	6.58 ± 0.63* (4.98 -8.19)	9.35 ± 0.04[b,c] (8.25 – 10.46)
$Ct.Ar/Tt.Ar^{S,T,S-T}$	0.32 ± 0.01 (0.30 – 0.34)	0.29 ± 0.01 (0.27 – 0.32)	0.32 ± 0.01 (0.30 – 0.35)	0.31 ± 0.01 (0.28 – 0.34)	0.31 ± 0.01 (0.28 – 0.33)	0.34 ± 0.01* (0.32 – 0.37)	0.38 ± 0.02*[,a] (0.32 – 0.44)	0.33 ± 0.01 (0.30 – 0.36)
$Tt.Ar/L^{S,T,S-T}$ (mm)	0.38 ± 0.01 (0.36 – 0.40)	0.41 ± 0.01 (0.38 – 0.45)	0.39 ± 0.01 (0.37 – 0.41)	0.40 ± 0.01 (0.38 – 0.42)	0.34 ± 0.01* (0.30 – 0.37)	0.32 ± 0.01* (0.31 – 0.34)	0.28 ± 0.02* (0.23 – 0.33)	0.36 ± 0.01*[,c] (0.33 – 0.38)
$Ec.Pm^{S}$ (mm)	16.16 ± 0.27 (15.49 – 16.83)	16.69 ± 0.27 (16.06 – 17.33)	16.96 ± 0.63 (15.32 – 18.60)	16.76 ± 0.31 (16.17 – 17.45)	15.07 ± 0.52 (13.64 – 16.50)	14.76 ± 0.27 (14.09 – 15.43)	16.14 ± 1.05 (13.43 – 18.85)	15.32 ± 0.30* (14.61 – 16.02)
$Ps.Pm^{S,T,S-T}$ (mm)	29.05 ± 0.38 (28.13 – 29.98)	30.29 ± 0.40 (29.34 – 31.24)	29.77 ± 0.45 (28.60 – 30.94)	29.93 ± 0.40 (29.04 – 30.81)	27.28 ± 0.69* (25.35 – 29.21)	26.22 ± 0.27* (25.55 – 26.89)	25.83 ± 0.54* (24.43 – 27.23)	27.63 ± 0.40*[,c] (26.68 – 28.58)
$J^{S,T,S-T}$ (mm^4)	20.53 ± 1.07 (17.92 – 23.13)	21.54 ± 0.74 (19.79 – 23.29)	21.48 ± 0.68 (19.82 – 23.14)	21.80 ± 0.65 20.37 – 23.22)	15.23 ± 0.81* (12.99 – 17.48)	15.32 ± 0.78* (13.40 – 17.24)	14.45 ± 1.01* (11.84 – 17.05)	17.73 ± 0.39*[,c] (16.82 – 18.65)
$Ecc^{S,T,S-T}$	0.48 ± 0.03 (0.41 – 0.55)	0.50 ± 0.02 (0.46 – 0.54)	0.56 ± 0.02 (0.50 – 0.62)	0.58 ± 0.02a (0.54 – 0.62)	0.48 ± 0.02 (0.42 – 0.55)	0.49 ± 0.03 (0.42 – 0.56)	0.45 ± 0.04* (0.34 – 0.56)	0.55 ± 0.02 (0.51 – 0.59)
$BS/BV^{S,S\_T}$ (mm^{-1})	7.89 ± 0.17 (7.48 – 8.30)	8.25 ± 0.10 (8.00 – 8.49)	7.79 ± 0.013 (7.44 – 8.13)	7.91 ± 0.20 (7.43 – 8.38)	8.78 ± 0.27* (8.04 – 9.52)	7.87 ± 0.24 (7.30 – 8.45)	8.15 ± 0.47 (6.94 – 9.35)	7.77 ± 0.17 (7.36 – 8.17)
TMD (gHA cm^{-3})	1.22 ± 0.03	1.24 ± 0.03	1.25 ± 0.02	1.27 ± 0.02	1.21 ± 0.02	1.24 ± 0.03	1.30 ± 0.03	1.28 ± 0.02

Data presented as mean ± standard error of the mean, data in brackets represents the lower and higher bounds of the 95% confidence interval.
[S] Significant effect of SCI, [T] significant effect of time post-surgery, [S-T] significant injury-time post injury interaction; ANOVA p<0.05.
** SCI different from SHAM at same timepoint post-surgery; p < 0.05.*
[a] Different from 2 weeks, [b] different from 6 weeks, [c] different from 10 weeks post-surgery; p<0.05.

Online Resource 10. 3D femoral mid-diaphyseal (58 - 62% bone length) cortical bone morphology and densitometry for SHAM and SCI rats at 2-, 6-, 10- and 16-weeks post-surgery.

	SHAM				SCI			
	2 Weeks (n = 8)	6 Weeks (n = 8)	10 Weeks (n = 8)	16 Weeks (n = 9)	2 Weeks (n = 8)	6 Weeks (n = 8)	10 Week s (n = 8)	16 Weeks (n = 8)
Ct.Th$^{S,T,S-T}$ (mm)	0.59 ± 0.01 (0.57 – 0.62)	0.67 ± 0.01^{a} (0.64 – 0.69)	0.74 ± 0.01^{a,b} (0.72 – 0.76)	0.79 ± 0.01^{a,b,c} (0.76 – 0.81)	0.52 ± 0.02* (0.48 – 0.57)	0.59 ± 0.01*^{,a} (0.57 – 0.60)	0.62 ± 0.01*^{,a} (0.58 – 0.66)	0.71 ± 0.01*^{a,b,c} (0.68 – 0.73)
Tt.Ar$^{S,T,S-T}$ (mm^2)	7.66 ± 0.22 (7.11 – 8.21)	9.22 ± 0.32^{a} (8.45 – 9.99)	9.03 ± 0.25^{a} (8.44 – 9.62)	9.30 ± 0.40^{a} (8.36 – 10.25)	7.78 ± 0.31 (7.00 – 8.57)	6.77 ± 0.34* (5.93 – 7.61)	6.96 ± 0.30* (6.20 – 7.73)	8.37 ± 0.33^{b,c} (7.60 - 9.14)
Ct.Ar$^{S,T,S-T}$ (mm^2)	4.65 ± 0.08 (4.46 – 4.84)	5.70 ± 0.11^{a} (5.45 – 5.96)	6.16 ± 0.14^{a} (5.84 – 6.49)	6.51 ± 0.21^{a,b} (6.02 – 7.00)	4.20 ± 0.14* (3.85 – 4.56)	4.20 ± 0.21* (3.69 – 4.70)	4.56 ± 0.17* (4.12 – 5.00)	5.64 ± 0.17*^{,a,b,c} (5.24 – 6.04)
Ma.Ar$^{S,T,S-T}$ (mm^2)	3.00 ± 0.18 (2.57 – 3.44)	3.51 ± 0.24 (2.93 – 4.09)	2.87 ± 0.13 (2.56 – 3.18)	2.79 ± 0.21 (2.29 – 3.29)	3.58 ± 0.27 (2.89 – 4.28)	2.58 ± 0.16*^{,a} (2.17 – 2.98)	2.40 ± 0.16*^{,a} (1.98 – 2.83)	2.73 ± 0.18^{a} (2.29 – 3.16)
Ct.Ar/Tt.Ar$^{S,T,S-T}$	0.61 ± 0.01 (0.58 – 0.64)	0.62 ± 0.01 (0.59 – 0.65)	0.68 ± 0.01 (0.67 – 0.70)	0.70 ± 0.01 (0.68 -0.73)	0.55 ± 0.02* (0.50 – 0.60)	0.62 ± 0.01 (0.59 – 0.65)	0.66 ± 0.01 (0.62 – 0.69)	0.68 ± 0.01 (0.65 – 0.71)
Tt.Ar/L$^{S,T,S-T}$ (mm)	0.23 ± 0.01 (0.21 – 0.25)	0.26 ± 0.01 (0.24 – 0.27)	0.25 ± 0.01 (0.23 – 0.27)	0.24 ± 0.01 (0.22 – 0.26)	0.23 ± 0.01 (0.20 – 0.26)	0.19 ± 0.01*^{,a} (0.17 – 0.22)	0.19 ± 0.01*^{,a} (0.17 – 0.20)	0.22 ± 0.01 (0.20 – 0.23)
Ec.Pm$^{S,T,S-T}$ (mm)	10.57 ± 0.15 (10.21 – 10.94)	11.63 ± 0.19^{a} (11.18 – 12.07)	11.56 ± 0.16^{a} (11.17 – 11.94)	11.72 ± 0.28^{a} (11.07 – 12.38)	10.66 ± 0.21 (10.12 – 11.20)	10.19 ± 0.18* (9.75 – 10.63)	10.02 ± 0.22* (9.46 – 10.59)	11.03 ± 0.19^{b,c} (10.57 – 11.49)
Ps.Pm$^{S,T,S-T}$ (mm)	17.36 ± 0.40 (16.37 – 18.34)	18.97 ± 0.43 (17.94 – 20.00)	18.34 ± 0.32 (17.58 – 19.11)	18.33 ± 0.54 (17.05 – 19.61)	17.99 ± 0.46 (16.80 – 19.18)	16.63 ± 0.35* (15.77 – 19.18)	16.02 ± 0.42*^{,a} (14.93 – 17.11)	17.54 ± 0.38 (16.64 – 18.44)
J$^{S,T,S-T}$ (mm^4)	8.05 ± 0.38 (7.11 – 8.98)	11.83 ± 0.66^{a} (10.27 – 13.40)	12.08 ± 0.64^{a} (10.56 – 13.60)	13.09 ± 1.02^{a} (10.67 – 15.51)	7.70 ± 0.49 (6.44 – 8.96)	7.09 ± 0.42* (6.07 – 8.12)	6.92 ± 0.57* (5.45 – 8.39)	10.26 ± 0.71*^{,a,b,c} (8.59 – 11.93)
Ecc$^{S,S-T}$	0.60 ± 0.02 (0.56 – 0.65)	0.62 ± 0.02 (0.56 – 0.67)	0.66 ± 0.01 (0.64 – 0.67)	0.66 ± 0.01 (0.64 – 0.69)	0.60 ± 0.01 (0.56 – 0.63)	0.61 ± 0.01 (0.59 – 0.64)	0.58 ± 0.01* (0.55 – 0.61)	0.58 ± 0.03* (0.52 – 0.65)
BS/BV^{S,T} (mm^{-1})	4.97 ± 0.09 (4.75 – 5.20)	4.56 ± 0.07^{a} (4.40 – 4.72)	4.24 ± 0.07^{a,b} (4.08 – 4.39)	4.01 ± 0.04^{a,b} (3.92 – 4.10)	5.61 ± 0.16* (5.19 – 6.03)	5.08 ± 0.09*^{,a} (4.87 – 5.29)	4.74 ± 0.09*^{,a} (4.52 – 4.96)	4.35 ± 0.05*^{,a,b,c} (4.22 – 4.48)
TMD (gHA cm^{-3})	1.33 ± 0.02	1.35 ± 0.01	1.36 ± 0.02	1.40 ± 0.02	1.31 ± 0.03	1.35 ± 0.02	1.37 ± 0.03	1.38 ± 0.02

Data presented as mean ± standard error of the mean, data in brackets represents the lower and higher bounds of the 95% confidence interval.
^{S} Significant effect of SCI, ^{T} significant effect of time post-surgery, $^{S-T}$ significant injury-time post injury interaction; ANOVA p<0.05.
** SCI different from SHAM at same timepoint post-surgery; p < 0.05.*
^{a} Different from 2 weeks, ^{b} different from 6 weeks, ^{c} different from 10 weeks post-surgery; p<0.05.

Online Resource 11. Three-point bend-derived whole-bone and material-level mechanical properties of the femur for SHAM and SCI rats at 2-, 6-, 10- and 16-weeks post-surgery.

	SHAM				SCI			
	2 Weeks (n = 7)	6 Weeks (n = 7)	10 Weeks (n = 7)	16 Weeks (n = 9)	2 Weeks (n = 8)	6 Weeks (n = 7)	10 Week s (n = 8)	16 Weeks (n = 8)
Rigidity (N/mm^2)^{S,T}	14512 ± 309	26818 ± 1385	36144 ± 1386^{a,b}	33597 ± 1718^{a,b}	10161 ± 875*	17105 ± 1022*	19610 ± 1256*	29612 ± 2005^{a,b,c}
Ultimate Moment (Nmm)^{S,T}	392,3 ± 23.3	543.4 ± 14.9^{a}	632.8 ± 12.3^{a}	630.3 ± 33.0^{a}	271.4 ± 7*	371.7 ± 5.1*	380.5 ± 1.0*	545.5 ± 30.3^{a,b,c}
Post-yield displacement (mm)^{S}	0.42 ± 0.02	0.40 ± 0.04	0.36 ± 0.04	0.31 ± 0.06	0.33 ± 0.03*	0.32 ± 0.01	0.30 ± 0.02	0.28 ±0.2
Energy-to-fracture (N)^{S,T}	12.8 ± 1.9	12.6 ± 0.8	11.3 ±0.6	11.1 ± 1.7	6.8 ± 0.6*	7.6 ± 0.3*	6.9 ± 0.2*	9.2 ± 1.1^{a}
Elastic Modulus (GPa)^{T}	4.31 ± 0.34	5.58 ± 0.38	7.67 ± 0.35^{a,b}	6.96 ± 0.56^{a}	3.42 ± 0.64	5.55 ± 0.56^{a}	6.74 ± 0.63^{a}	6.25 ± 0.70^{a}
Ultimate Stress (MPa)^{S,T}	160.3 ± 8.7	171.8 ± 5.8	196.0 ± 6.1^{a}	199.8 ± 9.7^{a}	124.8 ± 10.3*	171.7 ± 5.3^{a}	174.9 ± 6.9^{a}	194.5 ± 9.9^{a}

Data presented as mean ± standard error of the mean, data in brackets represents the lower and higher bounds of the 95% confidence interval.
^{S} Significant effect of SCI, ^{T} significant effect of time post-surgery, $^{S-T}$ significant injury-time post injury interaction; ANOVA p<0.05.
** SCI different from SHAM at same timepoint post-surgery; p < 0.05.*
^{a} Different from 2 weeks, ^{b} different from 6 weeks, ^{c} different from 10 weeks post-surgery; p<0.05.

Online Resource 12. Torsion-derived whole-bone and material-level mechanical properties of the femur for SHAM and SCI rats at 2-, 6-, 10- and 16-weeks post-surgery.

	SHAM				SCI			
	2 Weeks (n = 8)	6 Weeks (n = 8)	10 Weeks (n = 8)	16 Weeks (n = 9)	2 Weeks (n = 8)	6 Weeks (n = 8)	10 Weeks (n = 8)	16 Weeks (n = 8)
Rotational Stiffness (Nmm/θ)^{S,T}	1387 ± 54 (1259 – 1515)	1692 ± 145 (1337 – 2047)	2458 ± 130^{a,b} (2153 – 2764)	2971 ± 107^{a,b,c} (2719 – 3223)	636 ± 67* (477 – 795)	1078 ± 74*^{,a} (880 – 1275)	1281 ± 91*^{,a} (1065 – 1496)	1901 ± 116*^{,a,b,c} (1627 – 2176)
Ultimate Torque (Nmm)^{S,T}	334.9 ± 19.0 (290.0 – 379.8)	428.7 ± 38.1 (335.5 – 522.0)	486.1 ± 17.4^{a} (440.6 – 531.6)	595.0 ± 44.8^{a,b,c} (489.1 – 700.8)	198.1 ± 21.0* (148.6 – 247.7)	306.9 ± 12.8*^{,a} (274.8 – 339.0)	290.4 ± 18.2*^{,a} (247.3 – 333.4)	432.9 ± 15.4*^{,a,b,c} 396.4 – 469.3)
Energy-to-fracture (mJ)^{S,T}	54.1 ± 6.2 (39.5 – 68.6)	71.1 ± 11.1 (43.8 – 98.3)	60.2 ± 3.7 (50.5 – 70.0)	76.4 ± 11.1 (50.2 – 102.6)	48.5 ± 7.9 (29.8 – 67.1)	50.0 ± 3.8 (39.5 – 60.6)	38.5 ± 3.6* (30.0 – 47.1)	66.2 ± 8.2^{c} (46.8 – 85.5)
Rigidity Modulus (GPa)^{S,T}	2.11 ± 0.17 (1.85 – 2.38)	2.25 ± 0.18 (1.97 - 2.53)	3.33 ± 0.18^{a,b} (3.05 – 3.62)	4.07 ± 0.20^{a,b} (3.70 – 4.44)	1.60 ± 0.06* (1.51 – 1.68)	2.28 ± 0.24^{a} (1.90 – 2.66)	3.00 ± 0.21^{a} (2.65 – 3.34)	3.90 ± 0.35^{a,b,c} (3.39 – 4.40)
Ultimate Shear Stress (MPa)^{S,T}	70.7 ± 4.2 (60.5 – 81.0)	73.8 ± 2.6 (67.7 – 79.9)	78.6 ± 3.6 (73.2 – 84.0)	94.6 ± 6.7^{a,b} (83.7 – 105.5)	56.7 ± 3.6* (51.6 – 61.5)	70.4 ± 7.1 (60.1 – 80.6)	70.1 ± 4.6 (63.5 – 76.6)	83.7 ± 3.9^{a} (76.0 – 91.4)

Data presented as mean ± standard error of the mean, data in brackets represents the lower and higher bounds of the 95% confidence interval.
^{S} Significant effect of SCI, ^{T} significant effect of time post-surgery, $^{S-T}$ significant injury-time post injury interaction; ANOVA p<0.05.
** SCI different from SHAM at same timepoint post-surgery; p<0.05.*
^{a} Different from 2 weeks, ^{b} different from 6 weeks, ^{c} different from 10 weeks post-surgery; p<0.05.

Online Resource 13. Fourier Transform Infrared (FTIR) Spectroscopy-derived compositional parameter averages and spatial heterogeneity from proximal femoral diaphyseal cortical bone from 10-week post-surgery SHAM and SCI rats. MM: Mineral to Matrix ratio, CM: Carbonate to Mineral ratio, CP: Carbonate to Phosphate ratio, XLR: collagen cross-link ratio (collagen maturity) and APS: Acid Phosphate Substitution.

Average	MM	CM	CP	XLR	APS	Crystallinity
SHAM (n = 8)	8.86 ± 0.14 (8.52 – 9.20)	0.056 ± 0.002 (0.052 – 0.061)	0.006 ± 0.000 (0.006 – 0.007)	2.21 ± 0.03 (2.15 – 2.28)	0.49 ± 0.01 (0.47 – 0.50)	0.87 ± 0.01 (0.86 – 0.89)
SCI (n = 7)	8.96 ± 0.22 (8.42 – 9.51)	0.059 ± 0.002 (0.053 – 0.065)	0.007 ± 0.000 (0.006 – 0.007)	2.20 ± 0.02 (2.14 – 2.26)	0.48 ± 0.01 (0.47 – 0.49)	0.88 ± 0.01 (0.85 – 0.91)
Heterogeneity	**MM**	**CM**	**CP**	**XLR**	**APS**	**Crystallinity**
SHAM (n = 8)	5.35 ± 0.58 (3.96 – 6.74)	0.073 ± 0.010 (0.049 – 0.097)	0.007 ± 0.001 (0.004 – 0.010)	0.80 ± 0.07 (0.63 – 0.96)	0.15 ± 0.02 (0.11 – 0.20)	0.40 ± 0.06 (0.26 – 0.54)
SCI (n = 7)	5.24 ± 0.43 (4.18 – 6.30)	0.096 ± 0.021 (0.045 – 0.147)	0.008 ± 0.002 (0.004 – 0.012)	0.58 ± 0.03* (0.50 – 0.65)	0.14 ± 0.02 (0.10 – 0.18)	0.33 ± 0.05 (0.21 – 0.45)

Data presented as mean ± standard error of the mean, data in brackets represents the lower and higher bounds of the 95% confidence interval.
** SCI different from SHAM at 10-weeks post-surgery; p<0.05.*